

Functional regulation of the nuclear lamina
by SUMOylation pathway

「SUMO 化経路による核ラミナの機能調節機構」

2016

野 田 昂 文

兵庫県立大学大学院生命理学研究科

Contents

1. General Introduction	...3
2. Functional analysis of lamin A SUMOylation: SUMOylation-defective lamin A mutant associated with dilated cardiomyopathy induces cellular senescence.	
2-1. Summary	...4
2-2. Abbreviations	...4
2-3. Introduction	...5
2-4. Experimental procedures	...7
2-5. Results	...13
2-6 Discussion	...31
2-7 References	...34
3. Functional analysis of lamin A SIM: Requirement of lamin A SIM for lamin A reassembly at the end of mitosis	
3-1. Summary	...38
3-2. Abbreviations	...39
3-3. Introduction	...40
3-4. Experimental procedures	...43
3-5. Results	...47
3-6 Discussion	...67
3-7 References	...71
4. Acknowledgements	...76

1. General Introduction

The nuclear lamina is a fibrous structure located beneath the inner nuclear membrane that interacts with the nuclear pore complex (NPC), LEM (LAP2, emerin, MAN1)-domain proteins, which are integral proteins that are localized to the inner membrane of the nuclear envelope, and chromatin, thereby contributing both to nuclear structural stability and to regulation of chromatin organization in higher eukaryotes. The lamina is composed primarily of two types of lamins, A-type (lamin A/C) and B-type (lamin B1, B2) lamins, and lamin polypeptides have well-defined conserved domains, including an N-terminal head domain, a central α -helical rod domain, and a C-terminal tail domain. Both types of lamin proteins self-assemble into higher-order structures through multiple steps. First, the lamin polypeptides form a coiled-coil dimer through parallel association of two α -helical rod domains. Next, the lamin dimers associate in a head-to-tail fashion. Finally, intermediate filaments are formed by the interaction of these polymers in an antiparallel fashion. Although lamin A interacts with proteins involved in transcription, cell signaling and apoptosis, the regulatory mechanism of the interaction remains largely unknown. Interestingly, it is known that lamin A is modified with small ubiquitin-related modifier (SUMO; SUMOylation), which is well known to modulate protein-protein interaction.

SUMOylation is a modification that SUMO molecule covalently binds to lysine within the consensus sequence (Ψ KXE [Ψ : hydrophobic amino acids]). SUMOylation of proteins can mediate novel protein-protein interactions with other proteins containing SUMO-interacting motifs (SIMs). The SIM is a hydrophobic motif with a loose consensus sequence (V/L/I-X-V/L/I-V/L/I) that interacts non-covalently with the hydrophobic groove of SUMO. Interestingly, lamin A contains four SIM consensus sequences.

It is assumed that decrease of lamin A SUMOylation causes familial dilated cardiomyopathy (FDC). However, function of lamin A SUMOylation remains unknown and correlation between decrease of lamin A SUMOylation and FDC is not established. In Chapter 2, I describe possibility that decrease of lamin A SUMOylation are not a direct cause of FDC. In chapter 3, I describe the roles of SIM in lamin A.

2. Functional analysis of lamin A SUMOylation: SUMOylation-defective lamin A mutant associated with dilated cardiomyopathy induces cellular senescence.

2-1. Summary

Mutation of the lamin A gene causes a diverse range of diseases referred to as laminopathies. Because most laminopathies have a dominant inheritance pattern and progress gradually, cultured cells stably expressing mutant lamin A at the same level as the endogenous wild type cells are required for chronological analysis. In this study, I demonstrated that an expression system involving a lentiviral vector that carries the human metallothionein gene basal promoter ensures stable and basal level expression of proteins and is thus suitable for investigating the properties of lamin A mutants. The small ubiquitin-related modifier (SUMO) modification (SUMOylation)-defective E203G mutant that is associated with familial dilated cardiomyopathy exhibited abnormal sub-nuclear distribution and inhibited normal localization of WT lamin A in a dominant-negative manner. Low-level and long-term expression of the E203G mutant resulted in multinucleated giant cells, aberrant lipid droplet accumulation in the cytoplasm, and premature senescence. Expression of another SUMOylation-defective mutant (K201R) did not induce any phenotypes observed in cells expressing E203G. These results indicate that the E203G mutant may inhibit the normal functions of wild type lamin A in a dominant-negative manner, but a defect in SUMOylation itself may not be involved in disease pathogenesis. The K201R and E203G mutations decrease SUMOylation of lamin A.

2-2. Abbreviations

FDC, familial dilated cardiomyopathy; GRE, glucocorticoid responsive element; H3K9me3, histone H3 trimethylated on lysine 9; HFF, human foreskin fibroblast; hMT-IIA, human metallothionein-IIA; LMNA, lamin A gene; NEM, N-ethylmaleimide; SA β -gal, senescence-associated β -galactosidase; SUMO, small ubiquitin-related modifier; WT, wild type.

2-3. Introduction

The nuclear lamina is a fibrous structure beneath the inner nuclear membrane that interacts with both the nuclear membrane and chromatin, thereby contributing to nuclear structural stability and regulation of chromatin organization. The lamina is mainly composed of two types of lamins, A-type (lamin A/C) and B-type (lamin B1, B2). Lamin polypeptides have well-defined conserved domains, including an N-terminal head domain, a central α -helical rod domain, and a C-terminal tail domain (Parry et al., 1986). Both types of lamin proteins self-assemble into higher-order structures through multiple steps. First, the lamin polypeptides form a coiled-coil dimer through parallel association of two α -helical rod domains. Next, the lamin dimers associate in a head-to-tail fashion. Finally, intermediate filaments are formed by the interaction of these polymers in an antiparallel fashion (Dechat et al., 2010). Little information is available on the interaction between the A- and B-type lamins, although a recent fluorescence resonance energy transfer experiment demonstrated that both types of lamins interact with each other both homotypically and heterotypically in living cells (Delbarre et al, 2006). The expression patterns of the A- and B-type lamins differ between tissues, and the variations and combinations of lamin subtypes have been shown to play important roles in the regulation of tissue-specific gene expression.

Analysis of *Lmna*^{-/-} mice and *Lmna*^{-/-} mouse embryonic fibroblasts showed that lamin A plays important roles in chromatin organization, transcription regulation, DNA replication, and DNA repair. Approximately 300 mutations have been mapped to human *LMNA*. These mutations are associated with a wide range of heritable human diseases, collectively called laminopathies, including familial dilated cardiomyopathy (FDC), Emery-Dreifuss muscular dystrophy, familial partial lipodystrophy, and Hutchinson-Gilford progeria syndrome (Maraldi et al., 2010). Although several extensive investigations have evaluated cells with these *LMNA* mutations, the reason for different *LMNA* mutations causing different diseases and the precise molecular mechanisms underlying the lamin A-mediated regulation of various reactions in cell nuclei remain unclear. Defining the functions of lamin A has been difficult because fibroblasts isolated from patients with various laminopathies display similar phenotypes, including an aberrant nuclear structure, altered lamina assembly and chromatin structure,

downregulation of transcription, and resultant apoptosis (Broers et al., 2006). Furthermore, cultured cells transiently expressing mutant lamin A that is associated with laminopathy present a common abnormal nuclear structure and rarely exhibit any specific phenotype that could be attributed to each mutation. (Schreiber & Kennedy, 2013). Considering that most of the *LMNA* mutations that have been identified in patients are dominant mutations and that disease development takes a long time, culturing cells that stably express mutant lamin A at a level equivalent to that in endogenous wild type (WT) cells and the investigation of these cells over time is necessary. In this study, I employed a lentiviral vector carrying the human metallothionein-IIA promoter without the glucocorticoid responsive element (hMT-IIA[Δ GRE]) to ensure low-level and long-term expression of mutant lamin A. In this study, I investigated two lamin A mutants (K201R and the FDC-associated E203G), both of which carry a single amino acid substitution within the consensus sequence for small ubiquitin-like modifier (SUMO) modification (Ψ KXE [Ψ : hydrophobic amino acids]) and therefore are expected to be defective in SUMOylation. Indeed, previous experiments showed that lamin A is SUMOylated at K201 (Zhang & Sarge, 2008). Therefore, detailed analysis of cells expressing K201R mutation as well as E203G mutation may be important to understand direct correlation between the defect in SUMOylation and FDC pathogenesis. Our results revealed that both the K201R and E203G lamin A mutations indeed decrease SUMOylation at K201, as reported previously (Zhang & Sarge, 2008), but the distribution pattern in the nuclei of cells expressing these mutants was quite different. Moreover, only E203G lamin A inhibited normal localization of WT lamin A in a dominant-negative manner and decreased the amount of heterochromatin at the nuclear periphery. Long-term expression of E203G lamin A increased the accumulation of cytoplasmic lipid droplets and gradually induced premature senescence. Therefore, I propose that defects in lamin A SUMOylation are not a direct cause of FDC, but the E203 residue may be important for normal lamin A function. I also propose that development of a low-level and long-term expression system that harbors a lentivirus carrying the hMT-IIA basal promoter may be an appropriate approach to study late-onset laminopathies.

2-4. Experimental procedure

Cell culture

HeLa cells were cultured in Ham's F-12 medium containing 10% fetal bovine serum (FBS) (Nichirei Biosciences, Tokyo, Japan) at 37°C under 5% CO₂. HFF cells, a normal human foreskin fibroblast line immortalized by stable expression of the catalytic subunit of telomerase (Kiyono et al., 1998), and 293FT cells were maintained in DMEM (high glucose) supplemented with 10% FBS, 0.1 mM non-essential amino acid (GIBCO, Grand Island, NY, USA), 100 units/ml penicillin, 1 µg/ml streptomycin, 29.2 µg/ml L-glutamine and 100 µg/ml G418 (Promega, Madison, WI, USA) at 37°C under 5% CO₂.

Antibodies

A mouse anti-human lamin A/C monoclonal antibody was purchased from Santa Cruz. A rat anti-HA monoclonal antibody (clone 3F10) was purchased from Roche (Mannheim, Germany), and a mouse anti-FLAG monoclonal antibody (clone M2) was obtained from Sigma-Aldrich (St. Louis, MO, USA). Rabbit polyclonal anti-GFP antibody (632460) was purchased from Clontech (Mountain View, CA, USA). Rabbit polyclonal anti-histone H3K9me3 antibody (ab8898) was obtained from Abcam (Cambridge, MA, USA). Anti-rat and anti-mouse immunoglobulin G (IgG) species-specific antibodies linked to horseradish peroxidase (HRP) (NA935 and NA9310, respectively) were obtained from GE Healthcare Biosciences (Fairfield, CT, USA). Anti-rat and anti-mouse species-specific antibodies conjugated to Alexa Fluor 594 (A-11007 and A-11005) and Alexa Fluor 488 (A-11006 and A-11001) dyes from Life Technologies (Carlsbad, CA, USA). Anti-goat species-specific antibodies linked to Alexa Fluor 594 (A-21468) dye from Life Technologies.

cDNA cloning

cDNA for human lamin A and lamin B1 was amplified by PCR from a cDNA library prepared from HeLa cells. Base substitution mutations were introduced into the lamin A cDNA through site-specific mutagenesis employing the overlap extension method with combination of the appropriate oligonucleotides and confirmation by DNA sequencing. The primers used for cDNA amplification and mutagenesis were as follows;

WT lamin A, Forward: 5'- GGAGAATTCAGAGACCCCGTCCCAGCGGCG-3'

Reverse: 5'- GAAGGATCCTTACATGATGCTGCAGTTCTG-3'

lamin B1, Forward: 5'-CCGCTCGAGATGGCGACTGCGACCCCCGT-3'

Reverse: 5'-GTGCGGCCGCTTACATAATTGCACAGCTTC-3'

K201R lamin A, Forward: 5'-CAGACCATGAGGGAGGAACTGGACTT-3'

Reverse: 5'-CAGTTCCTCCCTCATGGTCTGCAGCC-3'

E203G lamin A, Forward: 5'-ATGAAGGAGGGACTGGACTTCCAGAA-3'

Reverse: 5'-GAAGTCCAGTCCCTCCTTCATGGTCT-3'.

Plasmids

Expression plasmids for FLAG-tagged WT, K201R, and E203G lamin A were generated by inserting lamin A cDNA between *EcoRI* and *BamHI* restriction sites of the pCSII-hMTIIA(Δ GRE)-FLAG-IRES2-Venus lentivirus vector containing the human metallothionein-IIA promoter (Fumoto et al., 2007) or pCSII-EF-HA-MCS-IRES2-Venus lentivirus vector containing the human EF1 α promoter. To construct CSII-hMTIIA(Δ GRE)-HA-lamin B1-IRES2-Venus for transient expression or lentivirus production, the lamin B1 cDNA was inserted between the *XhoI* and *NotI* sites of the CSII-hMTIIA(Δ GRE)-HA-MCS-IRES2-Venus lentivirus vector. Expression plasmids for CFP-SUMO2 and CFP-Ubc9 were described previously (Yamashita et al., 2004). Myc-SUMO2 expression plasmid was created by inserting cDNA encoding SUMO2 into pCMV5-myc plasmid.

Expression and purification of recombinant lamin A

cDNA encoding full-length WT or mutant human lamin A (amino acids 1–646) was inserted into a pET47b vector (Merck Millipore, Frankfurter Straße, Darmstadt, Germany); the cDNA was extended at the N-terminus using a 6 \times His tag followed by a HRV 3C protease cleavage site. The protein was expressed in *Escherichia coli* BL21 Codon Plus cells, which were harvested by centrifugation. The expressed lamin was extracted from the cells with gentle shaking in an extraction buffer containing 8 M urea, 100 mM NaH₂PO₄ (pH 8.0), and 10 mM Tris-HCl (pH 8.0) at room temperature for 4 h. After centrifugation at 100,000 \times g for 30 min at room temperature, the supernatant was mixed with Ni-NTA sepharose (Qiagen, Valencia, CA). After extensive washing of the resin with an extraction buffer at pH 7.0, the bound protein was eluted using an extraction buffer at pH 4.5. The eluate was dialyzed with buffer A containing 500 mM NaCl, 20 mM Tris-HCl (pH 8.0), and 1 mM DTT for 3 h, and the polyhistidine tag was removed using

HRV 3C protease (Merck Millipore) by overnight digestion at room temperature. Complete digestion and absence of non-specific cleavage were confirmed by SDS-PAGE. Samples were concentrated using Amicon Ultra 50k NMWL centrifugal filters (Merck Millipore) and subjected to Superdex 200 size exclusion chromatography (GE Healthcare) with buffer A. The peak fraction was used for electron microscopy analysis.

Paracrystal formation and EM

Purified lamin A at 1 mg/ml in buffer A was mixed with nine volumes of double-distilled water at room temperature. After 15 min of incubation, aliquots were absorbed onto glow-discharged carbon-coated copper grids, negatively stained with 2% uranyl acetate, and observed using a JEM1230 (JEOL) transmission electron microscope at an acceleration voltage of 100 kV.

Preparation and transduction of recombinant lentiviruses

Recombinant lentiviruses were produced as described previously (Yamashita et al., 2007). Briefly, 7 μg of the pCSII-hMTIIA(ΔGRE)-HA-IRES2-Venus plasmid containing cDNA for lamin A, 5 μg of pCAG-HIVgp, and 4 μg of pCMV-VSV-G-RSV-Rev were cotransfected into 293FT cells (3×10^6 cells/10-cm dish) using Lipofectamine 2000 reagent (Life Technologies). At 48 h after DNA transfection, the medium containing the recombinant lentiviruses was passed through a 0.45- μm filter and was used for viral transduction experiments. HFF cells and HeLa cells were transduced with lentivirus by adding an appropriate volume of virus-containing medium with polybrene at a final concentration of 6 $\mu\text{g}/\text{ml}$ for 6 h and washed with fresh medium three times. Cells stably expressing WT or mutant lamin A were cloned using the limiting dilution method. Virus transduction efficiencies were determined by counting GFP or Venus fluorescence-positive cells using an IX-70 fluorescence microscope (Olympus, Tokyo, Japan).

DNA transfection

For transient expression experiments, plasmid DNA transfection was conducted by the calcium phosphate method as described previously (Yamashita et al., 2004). Expression plasmids (3 μg in total) were added to 1×10^5 HeLa cells in 12-well plates. The medium was changed at 4 h after transfection, and the cells were cultured in fresh medium. In the case of 293FT cells, DNA transfection was performed using Lipofectamine 2000 (Life

Technologies) according to the manufacturer instructions. Cells were used for biochemical analysis and immunostaining at 48 h after DNA transfection.

Immunoprecipitation and Western blotting

Cells were washed with phosphate-buffered saline (PBS) and lysed in lysis buffer containing 20 mM HEPES (pH 7.4), 150 mM NaCl, 0.5% NP-40, 1 mM DTT, 0.1 mM EDTA, 20 mM N-ethylmaleimide (NEM), 1 mM Na₃VO₄, 5 mM NaF, 1 mM sodium pyrophosphate, and protease inhibitor cocktail (Roche) for 5 min on ice. The lysates were subjected to sonication (SHARP UT-106H) at 4°C and centrifugation at 15,000 × g for 20 min at 4°C. The supernatant was transferred to a new tube, and an anti-HA antibody (Roche) was added at a final concentration of 0.5 µg/ml. After incubation for 10 min at 4°C, a mixture of Dynabeads conjugated with protein G and Dynabeads conjugated with protein A (Life Technologies) (1/1, v/v) was added to the supernatant, and the tubes were rotated for 3 h at 4°C. The beads were washed with lysis buffer supplemented with 100 mM KCl five times and boiled in Laemmli sample buffer for 5 min. After brief centrifugation, the supernatants were subjected to SDS-PAGE and transferred to Immobilon-P membranes (Merck Millipore). Blots were incubated with the indicated primary antibodies in Tris-buffered saline (TBS) containing 5% skim milk and 0.05% Tween 20 and then with appropriate secondary antibodies conjugated with HRP. Bands were detected using an ECL kit (Thermo Scientific, Waltham, MA, USA). To quantify the relative amounts of endogenous and exogenous lamin A in HeLa and HFF cell lines, cells were harvested using cell scrapers, washed twice with ice-cold PBS, and lysed in CSK buffer (10 mM PIPES pH 6.8, 100 mM NaCl, 300 mM sucrose, 1 mM MgCl₂, and 1 mM EGTA) containing 0.1% Triton X-100. Equal amounts of protein were separated by SDS-PAGE and blotted onto Immobilon-P membranes. Both endogenous lamin A and HA-lamin A were detected using an anti-human lamin A/C antibody, and ECL signals were quantified using ImageJ. Protein concentrations were quantified using a protein assay kit (Bio-Rad, Hercules, CA, USA).

Immunofluorescence and fluorescence microscopy

Cells grown on glass coverslips were washed with PBS, fixed with 2% paraformaldehyde in PBS for 20 min, permeabilized in PBS containing 0.3% Triton X-100 for 15 min, and then blocked with 2% bovine serum albumin (BSA) in PBS. The coverslips were

incubated with the primary antibodies in TBS containing 0.1% BSA and 0.05% Tween 20 overnight at 4°C. After three washes with TBS containing 0.05% Tween 20, the coverslips were incubated with Alexa Fluor 488- or 594-conjugated secondary antibodies in TBS containing 0.1% BSA and 0.05% Tween 20 for 1 h at 4°C. For F-actin staining, Alexa Fluor 594-conjugated phalloidin (Life Technologies) was used according to the manufacturer instructions. DNA was stained using Hoechst 33258 dye. After two washes with PBS, the coverslip was mounted onto a glass slide spotted with ProLong Gold and SlowFade Gold Antifade Reagents (Life Technologies). The fluorescence was then visualized by confocal laser scanning immunofluorescence microscopy (LSM510 Zeiss) or fluorescence microscopy (Zeiss AX10). The fluorescence intensities of the images were quantified using ImageJ software.

BrdU labeling and detection

Labeling of proliferating cells with 5-bromo-2'-deoxyuridine (BrdU) was performed using the BrdU labeling and detection kit II (Roche) according to a partial modification of the manufacturer instructions. Briefly, cells were cultured in media containing 10 µM BrdU for 24 h and fixed with 70% ethanol/15 mM glycine (pH 2.0) for 20 min at -30°C. The coverslips were then covered with mouse anti-BrdU antibody (clone BMG 6H8) and nucleases for 30 min at 37°C. After three washes with PBS, the coverslips were incubated with Alexa Fluor 594-conjugated goat anti-mouse IgG species-specific antibody for 1 h at room temperature. After three washes with PBS, the coverslips were incubated with Alexa Fluor 594-conjugated chicken anti-goat IgG species-specific antibody at room temperature for 1 h. After three washes with PBS, the coverslips were incubated with rat anti-HA antibody (clone 3F10) overnight at 4°C. After three washes with PBS, the coverslips were incubated with AlexaFluor 488-conjugated goat anti-rat IgG species-specific antibody for 1 h at room temperature. The DNA was stained using Hoechst 33258 dye. After two washes with PBS, the coverslip was mounted onto a slide spotted with ProLong Gold and SlowFade Gold Antifade Reagents.

Lipid droplets staining and quantification of triacylglycerol

Cells were cultured with media containing 200 µM oleic acid complexed to 0.22% fatty acid-free bovine serum albumin (BSA; Sigma) for 24 h. The lipid droplets were stained with 0.1 mM BODIPY 493/503 dye (Life Technologies). Lipid extraction was performed

according to a standard procedure (Bligh & Dyer, 1959). TAG content was measured using the triglyceride E-test (WAKO). Protein concentration was estimated using a protein assay kit (Bio-Rad); BSA was used as a standard.

Trypan blue staining cell viability analysis

Cells were trypsinized and collected by centrifugation at $100 \times g$ for 10 min at 4°C. The cells were then suspended in PBS and an equal volume of 0.4% Trypan blue/PBS solution was added. The cell suspension was loaded into the counting chamber of a hemocytometer and the number of stained cells and total number of cells were immediately counted under the microscope. The percentage of stained cells was calculated by counting cells in five independent visual fields. Each field contained between 15 and 80 cells.

Senescence-associated β -galactosidase (SA β -Gal) assay

Cells were cultured on coverslips and fixed in PBS containing 2% formaldehyde and 0.2% glutaraldehyde for 20 min at room temperature, followed by three washes in PBS. Cells were immersed in freshly prepared SA β -gal staining solution containing 1 mg/mL 5-bromo-4-chloro-3-indolyl- β -D-galactoside in dimethylformamide, 30 mM citric acid/sodium phosphate buffer (pH 6.0), 5 mM potassium ferrocyanide, 5 mM potassium ferricyanide, 150 mM NaCl, and 2 mM MgCl₂ and incubated overnight at 37°C. The coverslips were washed three times with PBS and mounted on glass slides with Glycergel Mounting Medium (Dako, Glostrup, Denmark).

Statistical analysis

Statistical significance was determined using Student's t test. $p < 0.05$ was considered to be statistically significant.

2-5. Results

To investigate the effect of the K201R and E203G mutations on SUMOylation of the lamin A polypeptide, I performed an *in vivo* SUMOylation assay. HeLa cells were co-transfected with hemagglutinin (HA)-lamin A expression plasmids together with cyan fluorescent protein (CFP)-SUMO2 and CFP-Ubc9 expression plasmids. Cell lysates were prepared and subjected to immunoblot analysis 48 h after DNA transfection (Fig. 1A). Anti-HA antibodies detected a signal of high molecular weight in addition to the signal corresponding to the 75-kDa HA-tagged WT (HA-WT) lamin A in the lysate of cells co-expressing CFP-SUMO2 and CFP-Ubc9. Separation of the polypeptides in a 7.5% polyacrylamide gel revealed that the apparent molecular mass of this slow-migrating band was as 180 kDa. This 180 kDa signal was scarcely detected in the lysate from cells expressing the K201R lamin A and E203G mutant, suggesting that the 180 kDa band represented SUMOylated lamin A. To confirm this finding, I performed immunoprecipitation experiments (Fig. 1B). Cells transfected with expression plasmids for HA-lamin A, CFP-SUMO2, and CFP-Ubc9 were subjected to immunoprecipitation using an anti-HA antibody followed by immunoblotting with an anti-green fluorescent protein (GFP) antibody. The anti-GFP antibody detected the 180 kDa band, indicating that the 180 kDa polypeptide may correspond to SUMOylated HA-lamin A, as reported previously (Zhang & Sarge, 2008). The apparent molecular mass of SUMOylated lamin A was much higher than the estimated molecular mass of the HA-lamin A polypeptide with a single-molecule CFP-SUMO2 conjugation. Similar result was also obtained *in vivo* SUMOylation assay using myc-SUMO expression plasmid instead of CFP-SUMO plasmid (Fig. 1C). The apparent molecular mass of the slow-migrating HA-lamin A polypeptide detected in the extract from cells co-expressing myc-SUMO2 and CFP-Ubc9 was estimated to be 145 kDa. This phenomenon was also observed in lamin A as reported by Zhang and Sarge (Zhang & Sarge, 2008) and in other SUMOylation substrates (Hietakangas et al., 2003; Kotaja et al., 2002; Sapetschnig et al., 2002; Subramanian et al., 2003).

The intranuclear localization patterns of K201R and E203G are different

Because SUMOylation has been shown to cause changes in the subcellular localization of target proteins (Gill, 2004), I investigated the effect of the K201R and

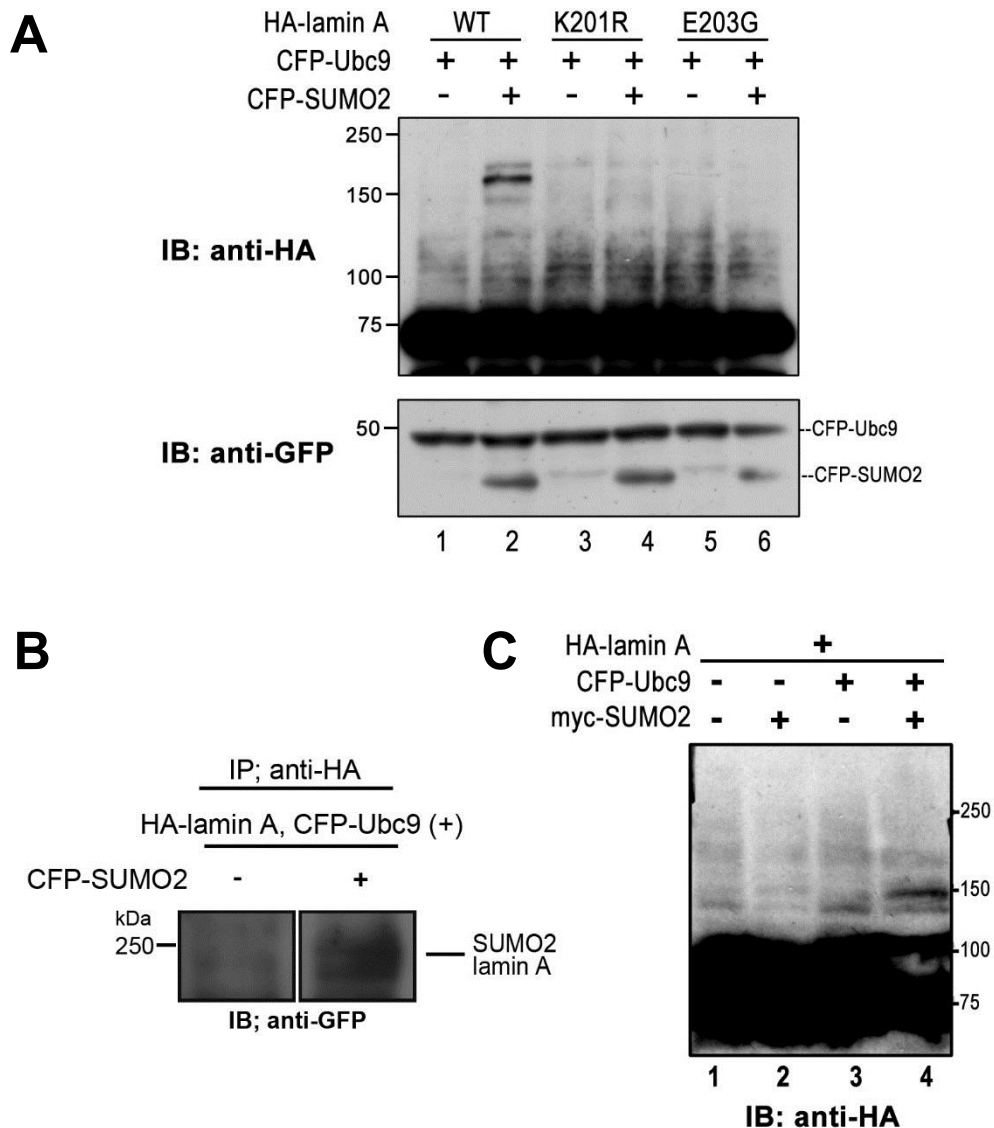


Figure 1. Decrease in SUMOylation of lamin A by K201R and E203G mutation. (A) HeLa cells were transfected with plasmids expressing the indicated proteins and directly lysed in boiled Laemmli sample buffer. Polypeptides in whole cell lysates were separated in a 7.5 % SDS polyacrylamide gel and subjected to western blot analysis using anti-HA and anti-GFP antibodies. (B) HeLa cells were transfected with plasmids expressing the indicated proteins and lysed in lysis buffer containing N-ethylmaleimide (NEM). HA-lamin A was immunoprecipitated using an anti-HA antibody and then SUMOylated HA-lamin A polypeptides were detected by western blot analysis using anti-GFP antibodies. (C) 293FT cells were transfected with plasmids expressing the indicated proteins and directly lysed in boiled Laemmli sample buffer. Polypeptides in whole cell lysates were separated in a 10 % SDS polyacrylamide gel and subjected to western blot analysis using anti-HA antibodies.

E203G mutations on lamin A distribution. Two types of expression drivers, the human metallothionein IIA (hMT-IIA[Δ GRE]) promoter and the human elongation factor-1 alpha (EF1 α) gene promoter, were adopted for low-level (Fumoto et al., 2007) and high-level expression (Nelson et al., 2010; Ye et al., 1998), respectively, because the overexpression of proteins occasionally results in aggregates or causes mislocalization of proteins. HeLa cells were simultaneously transfected with WT, K201R, or E203G HA-lamin A expression plasmids and CFP-Ubc9 with or without the CFP-SUMO2 plasmid. Immunoblot analysis with an anti-lamin A/C antibody revealed that the amount of exogenous HA-lamin A expressed by the hMT-IIA(Δ GRE) promoter and that expressed by the EF1 α promoter were approximately 1.6- and 3.4-fold higher than the amount of endogenous lamin A, respectively (Fig. 2A), and slower migrating signals were not detected under this condition. I assume that failure in detecting the slower migrating signals using anti-lamin A/C monoclonal antibody was due to its low binding affinity to the antigen because anti-HA antibody certainly visualized the slower migrating signals as shown in Fig. 1A. The subcellular localization of HA-lamin A expressed by the hMT-IIA(Δ GRE) and EF1 α promoters, determined using an anti-HA antibody, is shown in Fig. 2B and Fig. 2C, respectively. WT and K201R lamin A were normally localized at the nuclear periphery regardless of the promoter used. In contrast, the distribution pattern of E203G lamin A unexpectedly depended on the promoter type. E203G lamin A expressed by the hMT-IIA(Δ GRE) promoter was widely distributed inside the nuclei in addition to at the nuclear periphery, whereas many small aggregates were observed along the nuclear membrane when E203G lamin A was expressed by the EF1 α promoter (Fig. 2C), as described in previous reports (Lloyd et al., 2002; Zhang & Sarge, 2008). Considering that the cytomegalovirus major immediate-early promoter/enhancer, a commonly used strong driver, was used in both previous studies, I speculate that accumulation of E203G lamin A beyond a certain threshold limit may have resulted in the formation of aggregates in the nuclei. Therefore, I decided to use the vector carrying MT-IIA(Δ GRE) to express lamin A in all subsequent experiments. Unexpectedly, the distribution patterns of WT, K201R, and E203G lamin A did not appear to change upon co-expression with CFP-SUMO2, suggesting that SUMOylation of lamin A is not involved in the regulation of the subcellular localization of lamin A.

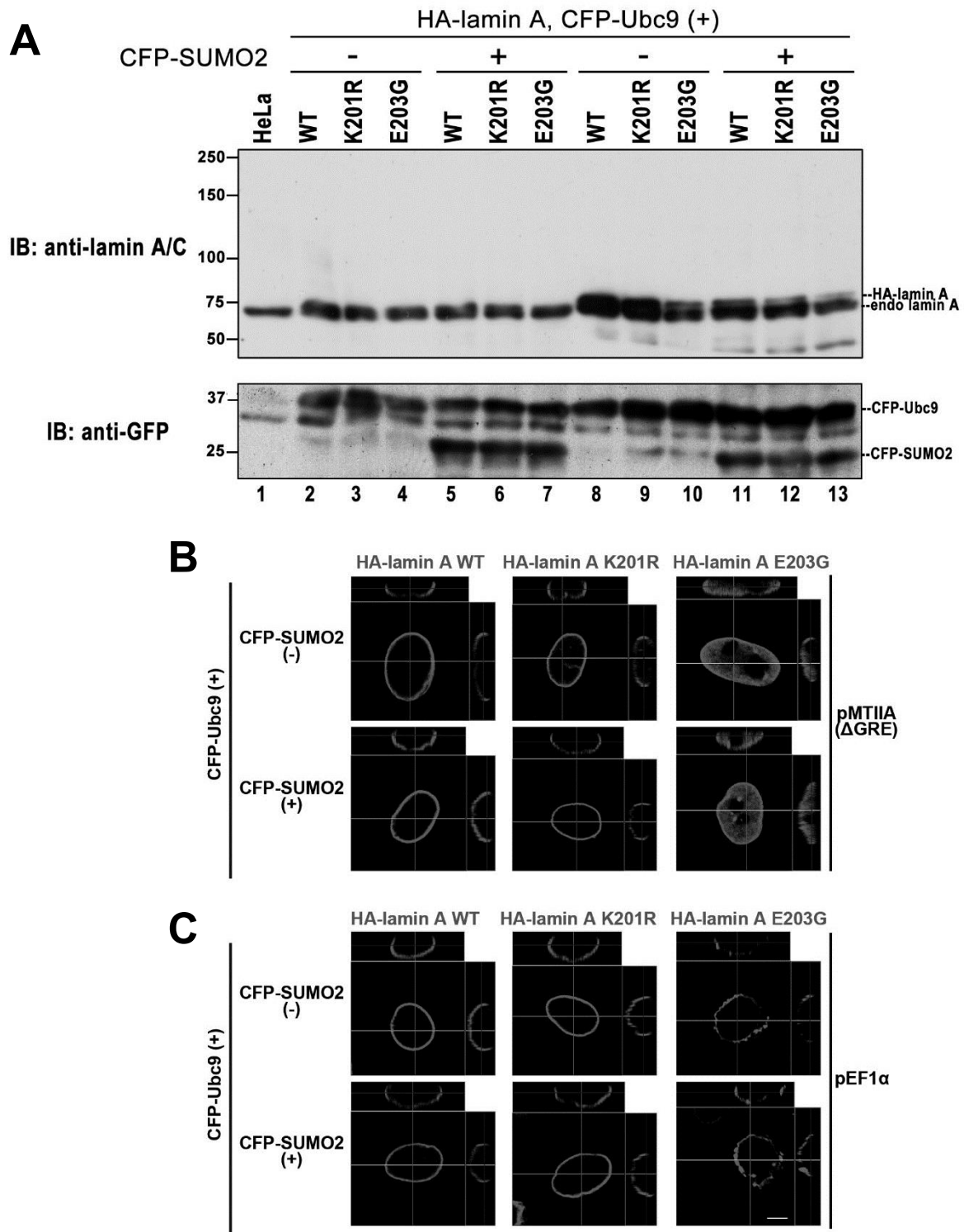


Figure 2. Different localization of WT, K201R and E203G lamin A. (A) HeLa cells were transfected with expression plasmids as indicated, and directly lysed in boiled Laemmli sample buffer. HA-lamin A polypeptides were detected by western blotting analysis using anti-HA antibody. HA-lamin A was expressed under the control of the hMTIIA(Δ GRE) promoter (lanes 2-7) and EF1 α promoter (lanes 8-13). (B and C) HeLa cells were transfected with plasmids expressing HA-lamin A, CFP-SUMO2 and CFP-Ubc9 and stained with an anti HA-antibody. HA-lamin A signals were visualized by confocal fluorescence microscopy. Expression of HA-lamin A was driven by hMTIIA(Δ GRE) promoter (B) or EF1 α promoter (C). Bar, 5 μ m.

K201R and E203G lamin A formed paracrystals in in vitro studies

Lamin A belongs to the type V intermediate filament family and assembles into higher order structures *in vivo* and *in vitro* (Stuurman et al., 1998). Because the E203G mutation lies between the two α -helical rod domains that are involved in coiled-coil dimer formation, I speculate that the E203G mutation destroys or weakens the homodimer formation ability of lamin A. To examine this possibility, I obtained recombinant WT and mutant lamin A, and then compared their ability to form paracrystals. In this study, I expressed the mature form (646 amino acids) of both WT and mutant lamin A in bacteria (Weber et al., 1989), purified them to homogeneity, and used the purified lamins to investigate paracrystal formation under conditions of reduced salt concentrations (Stuurman et al., 1998). The resultant paracrystals were negatively stained with uranyl acetate and then detected by transmission electron microscopy (Fig. 3). The sizes and shapes of the paracrystals and their typical stripe patterns did not differ between the three constructs.

E203G lamin A interferes with the normal distribution of WT lamin A in a dominant-negative manner

Both the K201R and E203G mutants apparently formed paracrystals *in vitro*. Next, I evaluated whether these mutants could interact between themselves and/or with WT lamin A *in vivo*. To test the interaction between WT and mutant lamin A, HA-tagged and FLAG-tagged lamin A (WT, K201R, and E203G) were simultaneously expressed in HeLa cells, and the association between HA- and FLAG-lamin A were examined by immunoprecipitation using an anti-HA antibody followed by immunoblotting using an anti-HA or anti-FLAG antibody. As shown in Fig. 4A, both K201R and E203G were associated with WT-lamin A. In addition, there was no substantial difference among binding affinities between WT-WT, WT-mutant, and mutant-mutant interactions regardless of the absence or presence of CFP-SUMO2. SUMOylated lamin A was not detected in immunoprecipitates, presumably due to its low amount or deSUMOylation during sample preparation. This result suggests that the E203G and K201R lamin A mutants associate with WT lamin A and between themselves *in vivo*.

The association of E203G lamin A with WT lamin A raises the possibility that expression of E203G lamin A may impair the normal localization of WT lamin A. To test

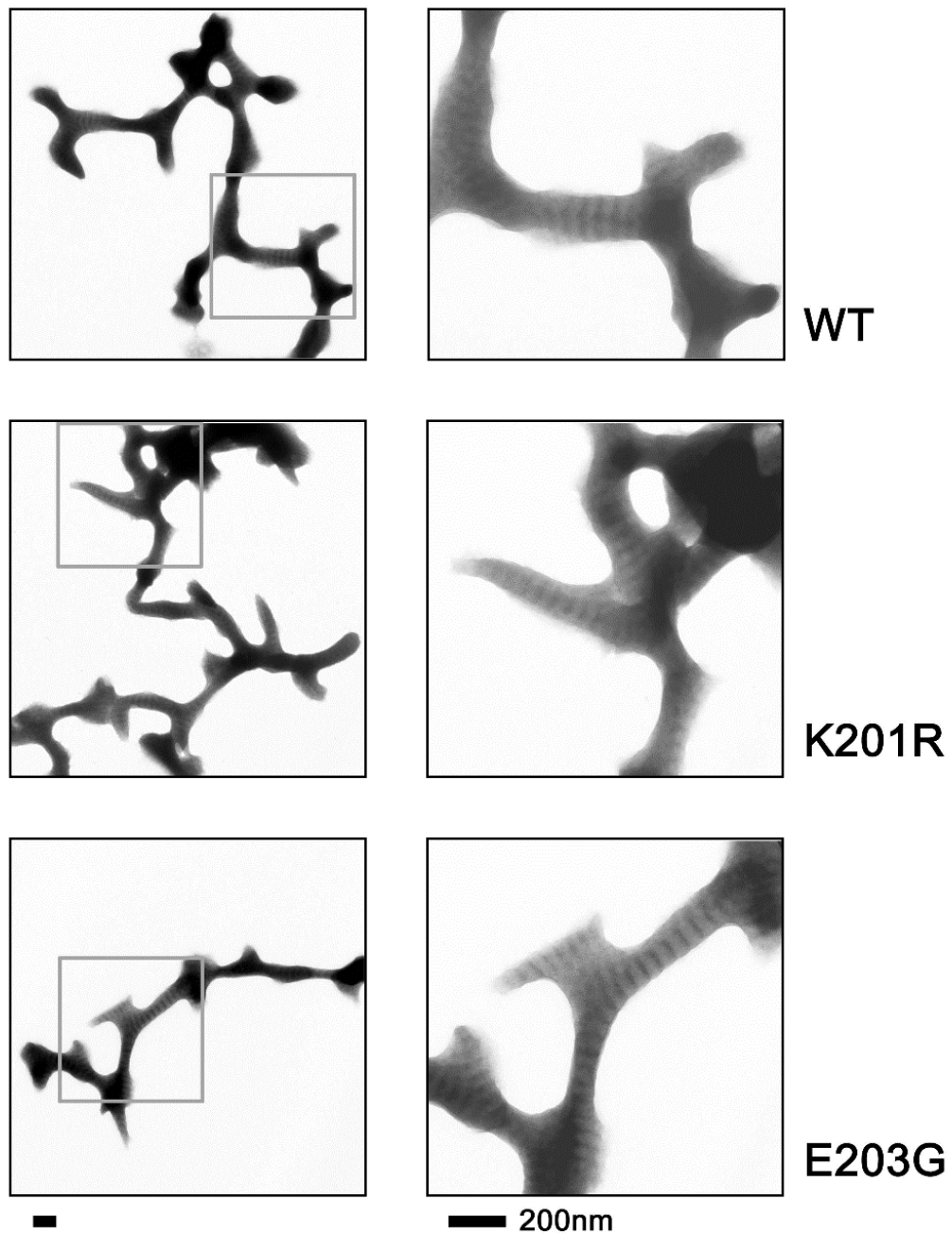


Figure 3. Structural analysis of paracrystals assembled from purified WT, K201R, and E203G lamin A proteins. Bacterially expressed and purified WT, K201R and E203G lamin A proteins were allowed to self-assemble into paracrystals in vitro, were negatively stained, and were analyzed by transmission electron microscopy.

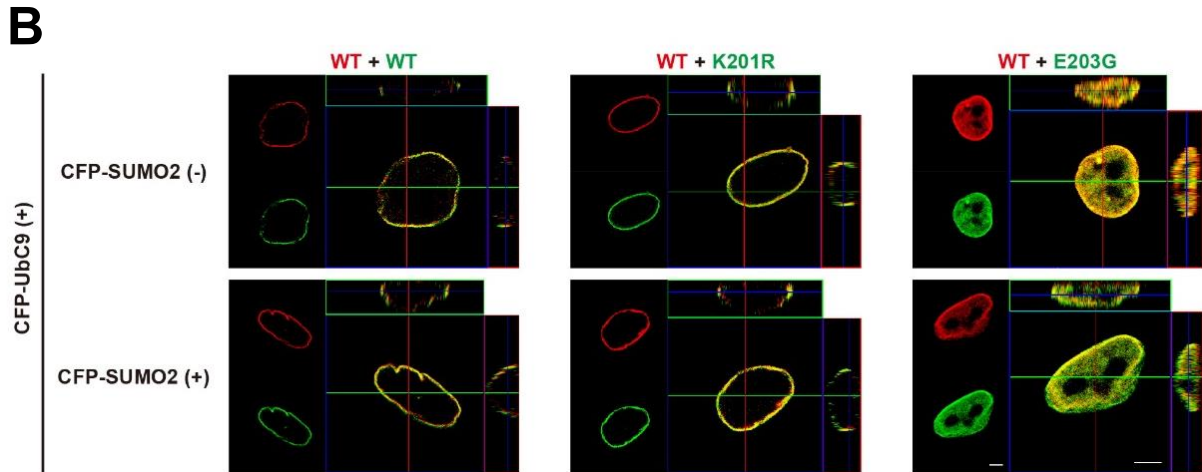
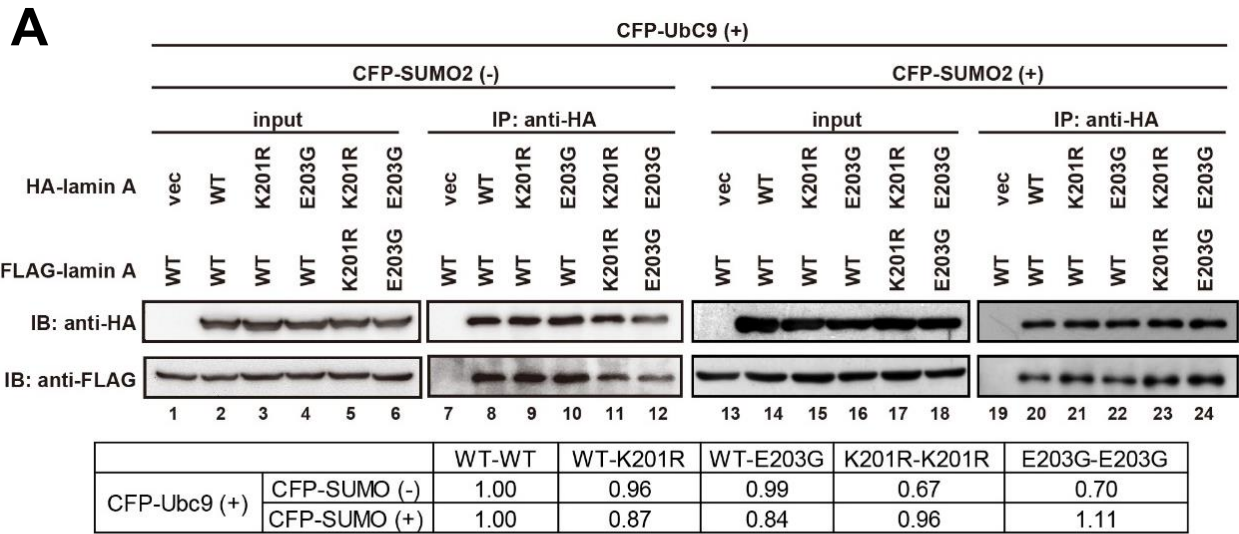


Figure 4. Dominant-negative inhibition of localization by E203G lamin A. (A) 293FT cells were transfected with plasmids expressing the indicated proteins and lysed in lysis buffer containing 20 mM NEM. HA-lamin A was immunoprecipitated using an anti-HA antibody. HA- and FLAG-lamin A polypeptides were detected by western blotting analysis using anti-HA and anti-FLAG antibodies, respectively. Relative amounts of immunoprecipitated HA-lamin A and co-immunoprecipitated FLAG lamin A were determined by quantifying the signals using ImageJ. Binding affinity between HA- and FLAG-lamin A was defined as a ratio of FLAG-lamin A/ HA-lamin A. Binding affinities between the combinations of lamin A indicated were shown as values relative to that of WT-WT in the table. (B) HeLa cells were transfected with plasmids expressing HA-lamin A, FLAG-lamin A, CFP-SUMO2 and CFP-Ubc9. HA-lamin A (green) and FLAG-lamin A (red) were immunostained and visualized by confocal fluorescence microscopy. Bar, 5 μ m.

this hypothesis, HeLa cells were co-transfected with FLAG-tagged and HA-tagged WT, K201R, and E203G lamin A, and the distribution of lamin A was determined by immunostaining (Fig. 4B). A large portion of WT lamin A was abnormally localized inside the nuclei together with E203G lamin A, indicating that E203G lamin A may interfere with the normal localization of WT lamin A in a dominant-negative manner.

E203G mutant lamin A does not affect the normal localization of lamin B1

Interaction between lamin A and lamin B1 has been demonstrated by yeast two-hybrid (Ye & Worman, 1995) and fluorescence resonance energy transfer experiments. Many studies have shown that a set of *LMNA* mutations in association with progerin impaired the normal distribution of lamin B1 (Delbarre et al., 2006). Therefore, immunoprecipitation experiments were conducted to examine the interaction between E203G and K201 R lamin A and lamin B1. As shown in Fig. 5A, the K201R and E203G lamin A mutants, and WT lamin A co-immunoprecipitated with lamin B1 regardless of whether CFP-SUMO2 was simultaneously expressed. I then examined the effects of K201R and E203G lamin A on the subcellular localization of lamin B1. The results revealed that low-level and transient expression of K201R and E203G did not affect the normal localization of lamin B1, as shown in Fig. 5B.

Transient expression of E203G lamin A impairs peripheral heterochromatin formation

Several lines of evidence suggest that lamin A is involved in the formation of heterochromatin, especially at the nuclear periphery (Shumaker et al., 2006; Solovei et al., 2013). To examine the effect of the expression of K201R and E203G lamin A on heterochromatin formation, heterochromatin in HeLa cells expressing E203G lamin A was visualized using an antibody targeting the trimethylation at the lysine 9 (K9) residue of histone H3 (H3K9me3; Fig. 6A). Peripheral heterochromatin was observed in control HeLa cells and in HeLa cells overexpressing WT or K201R lamin A (Fig. 6A, B). In contrast, cells expressing E203G lamin A exhibited a loss of H3K9me3 fluorescence at the nuclear periphery (Fig. 6A, B). Quantification of the H3K9me3 signals showed a statistically significant reduction of heterochromatin signals at the nuclear periphery in E203G-expressing cells (Fig. 6C), indicating that E203G lamin A may have lost the activity responsible for peripheral heterochromatin formation.

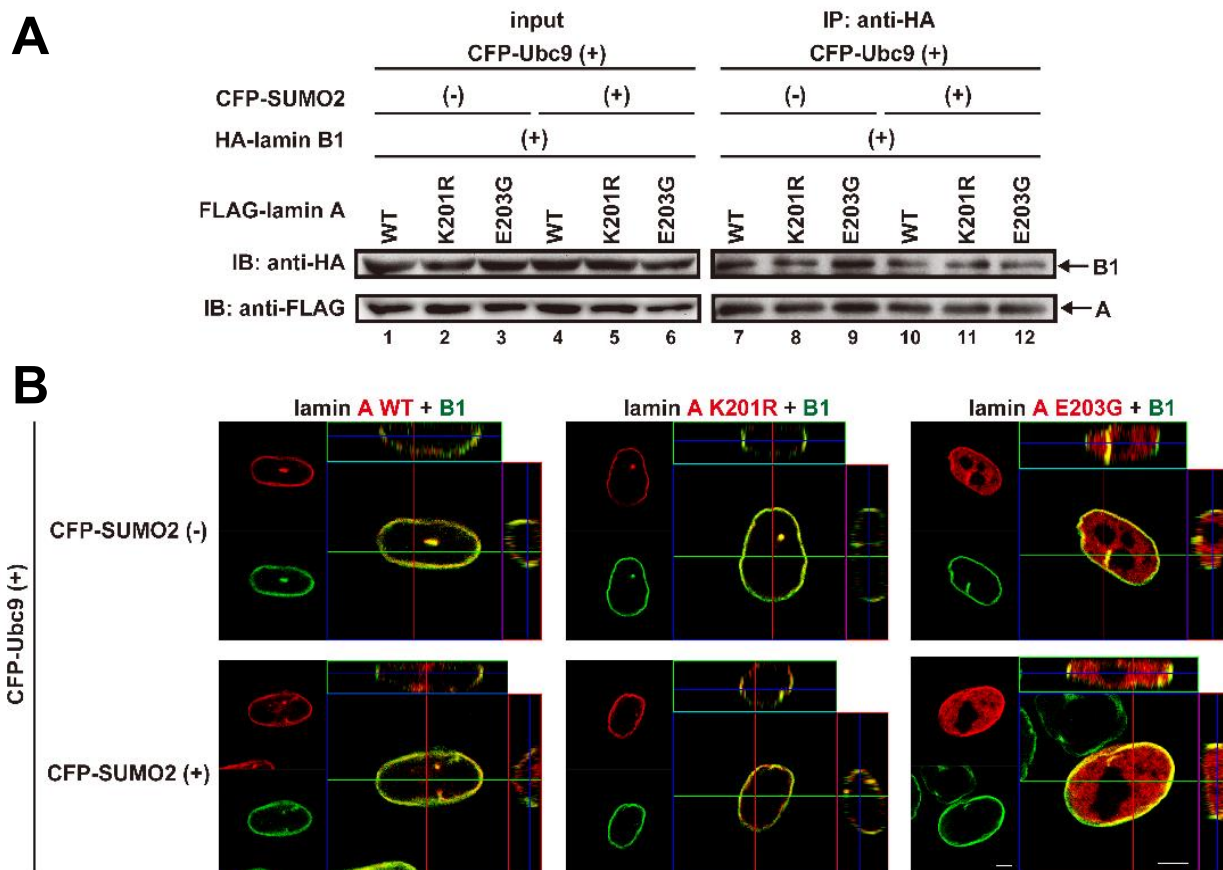


Figure 5. Effect of E203G lamin A expression on localization of lamin B1. (A) 293FT cells were transfected with plasmids expressing the indicated proteins. HA-lamin B1 was immunoprecipitated using an anti-HA antibody. HA-lamin B1 and FLAG-lamin A (WT, K201R or E203G) were detected by western blotting analysis using anti-HA and anti-FLAG antibodies, respectively. (B) HeLa cells were transfected with plasmids expressing HA-lamin B1, FLAG-lamin A (WT, K201R or E203G), CFP-SUMO2 and CFP-Ubc9. HA-lamin B1 (green) and FLAG-lamin A (red) were visualized by confocal microscopy. Bar, 5 μ m.

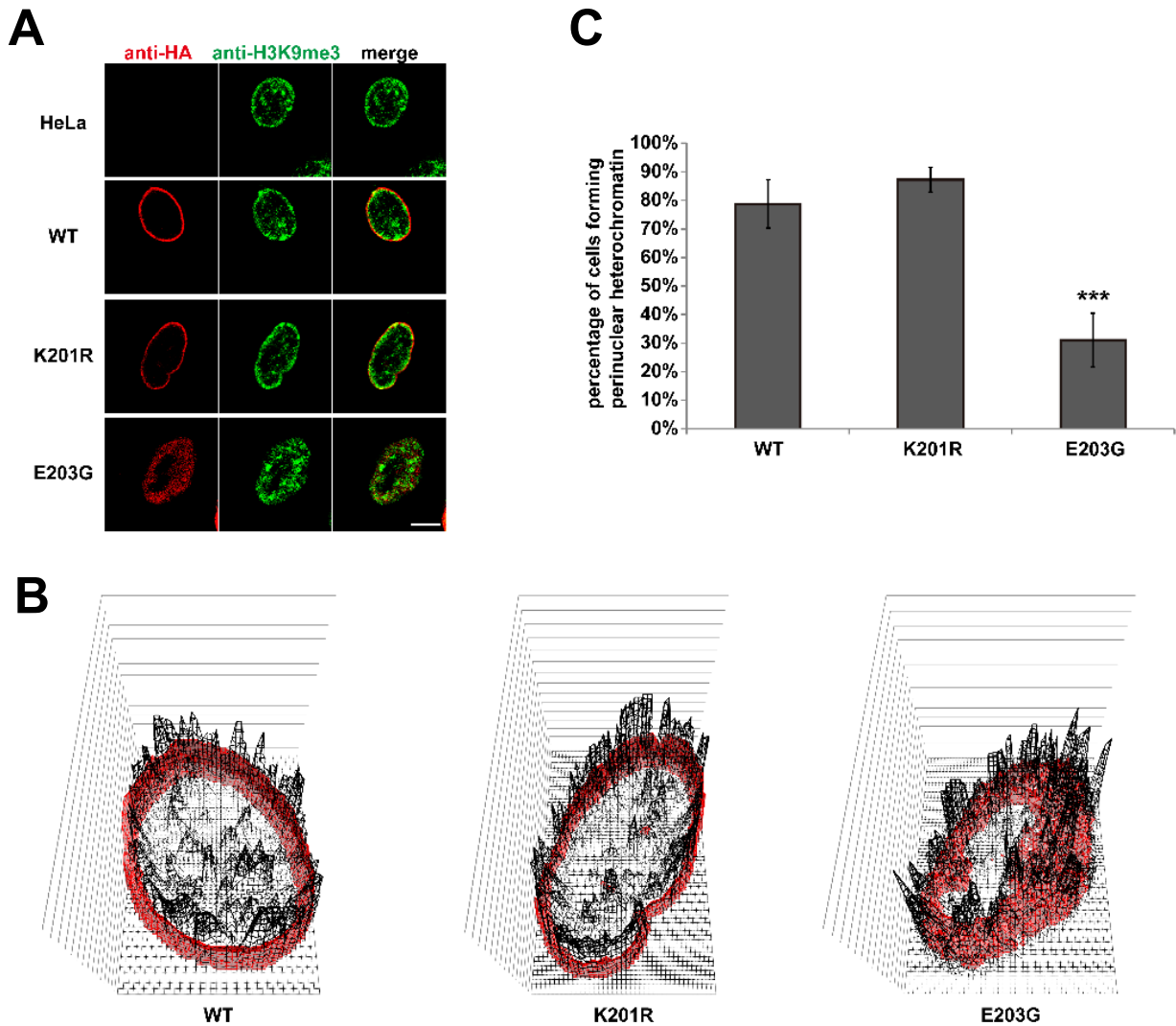


Figure 6. Expression of E203G lamin A decreases peripheral heterochromatin. (A) HeLa cells were transfected with plasmids expressing HA-lamin A (WT, K201R or E203G), CFP-SUMO2 and CFP-Ubc9. At 48 h after transfection, cells were stained using anti-HA (red) and anti-H3K9me3 (green) antibodies. Bar, 5 μ m. (B) HA and H3K9me3 fluorescence signals on images in Fig.5A were quantified using ImageJ software and are shown as a 3D graph. The z-axis indicates the intensity of fluorescence. Black and red lines indicate the intensity of green fluorescence (H3K9me3 signal) and red fluorescence (HA-lamin A) signal, respectively. (C) Quantitative analysis of cells forming peripheral heterochromatin (>45 cells were analyzed). Data are shown as means \pm SEM. (***, $p < 0.0005$ vs. WT) and represent two separate experiments.

Multinucleated giant cells induced by long-term expression of E203G lamin A ceased to proliferate

Given that cardiomyopathy induced by the E203G mutation takes decades to develop, I generated HeLa cell lines stably expressing lamin A and investigated their phenotypes over a long period. HeLa cells were transduced with a lentiviral vector harboring cDNA encoding WT, K201R, and E203G lamin A at a multiplicity of infection of approximately 0.3, and cell lines were then established using the limiting dilution method. The cellular morphology of the obtained cell lines was observed by F-actin staining (Fig. 7A). The expression level of exogenous HA-lamin A in each cell line expressing WT, K201R, or E203G lamin A was similar to that of endogenous lamin A (Fig. 7C and Fig. 10A) and no slower migrating signal was detected using anti-lamin A/C antibody. Multinucleated cells and giant cells appeared in HeLa cell lines stably expressing E203G lamin A, but not in the control cell lines transduced with the empty vector or in cell lines stably expressing WT or K201R lamin A (Fig. 7D). As shown in the lower panel of Fig. 7B, bridge-like structures connecting two nuclei were often observed. Trypan blue exclusion revealed decreased viability in the cell line expressing E203G lamin A (Fig. 7E). To determine when multinucleated or giant cells emerge, cellular morphology was monitored over 1 month after the lentivirus expressing E203G lamin A was transduced into HeLa cells (Fig. 7F). The number of cells exhibiting abnormal morphology did not significantly increase in the first couple of days. However, the population of aberrant morphological cells gradually increased 1 week after virus transduction and reached a maximum (approximately 6%) level after 1 month.

To determine whether the multinucleated cells proliferated, 5-bromo-2'-deoxyuridine (BrdU) was added to the cells 21 days after virus transduction, and BrdU-incorporating cells were detected using an anti-BrdU antibody. Under these conditions, 93.7% of the HA-E203G lamin A-negative cells were labeled with BrdU. In contrast, 12.2% of the multinucleated giant cells and 51.5% of the cells with normal morphology expressing HA-E203G lamin A incorporated BrdU (Fig. 7G). It should be noted that the BrdU signal was significantly reduced in HeLa cells with HA-lamin A signals. These results indicate that overexpression of E203G lamin A reduced cell proliferation and that the multinucleated giant cells ceased to proliferate.

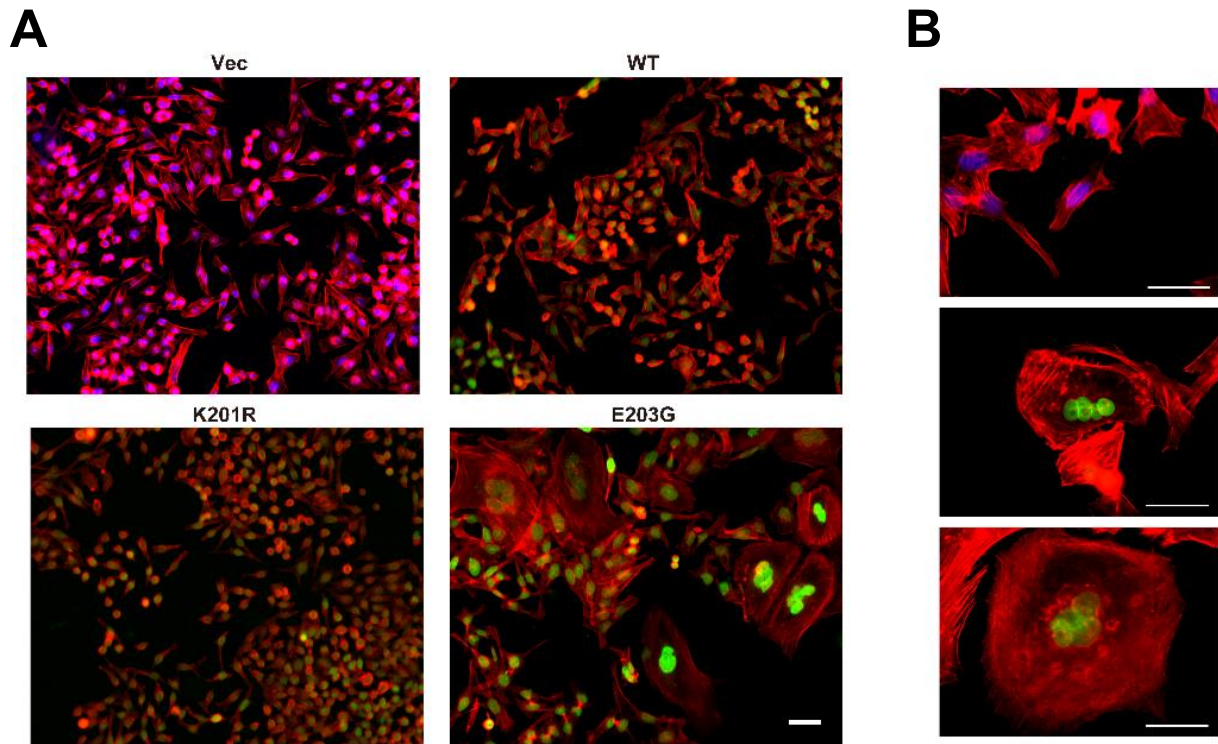


Figure 7. Multinucleated giant cells emerge after long-term expression of E203G lamin A. (A and B) (A) HeLa cell lines obtained by transduction of lentiviruses carrying empty vector (Vec) or expressing HA-WT, K201R or E203G were stained with anti-HA antibody (green) and Alexa Fluor 594-phalloidin and visualized by a fluorescence microscopy at low magnification (100×). (B) Images at high (400×) magnification. Upper panel, control HeLa cell line transduced with an empty virus; middle and lower panels, HeLa cell line expressing E203G lamin A. Bar, 50 μm.

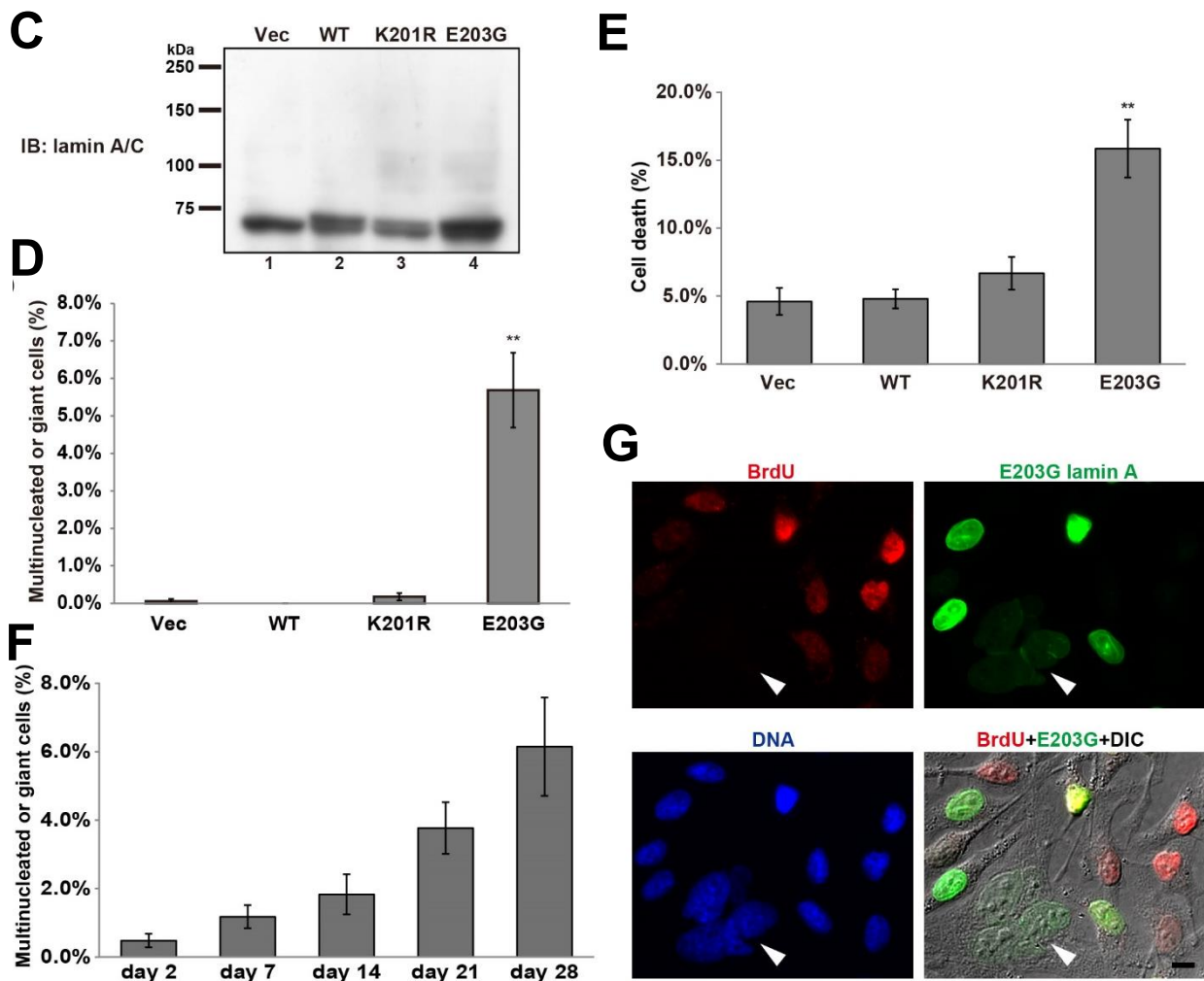


Figure 7. Multinucleated giant cells emerge after long-term expression of E203G lamin A. (C) The amount of endogenous and HA-lamin A expressed in each cell line at approximately 1 month after virus transduction used in Fig. 7A, B, D, and E was determined by western blotting analysis using an anti-lamin A/C antibody. Equal amounts of protein were loaded in each lane. Approximately 100 kDa signals were non-specific bands. (D) The percentage of multinucleated or giant cells in cell lines transduced by lentiviruses carrying an empty vector (Vec) or expressing HA-WT, K201R, or E203G lamin A was calculated. Data are shown as the mean \pm SEM. (**, $p < 0.005$ vs. Vec). More than 500 cells were scored in three independent images. (E) The rate of cell death in cell lines transduced by lentivirus carrying empty vector (Vec) or expressing WT, K201R, or E203G was calculated by Trypan blue exclusion assay. Data are shown as the mean \pm SEM. (**, $p < 0.005$ vs. Vec) More than 150 cells were scored in eight independent images. (F) Multinucleated or giant cells in the HeLa cell population transduced by lentiviruses expressing E203G lamin A were counted from day 2 to day 28. More than 4000 cells were scored in three independent images. (G) HeLa cells were transduced with lentiviruses expressing E203G lamin A. At 20 days after viral transduction, cells were cultured in media containing 10 μ M BrdU for 24 h, then fixed and immunostained with an anti-BrdU antibody. Cells expressing E203G lamin A were detected by their GFP signal. A multinucleated cell is indicated by the arrowhead. Bar, 10 μ m.

Long-term expression of E203G lamin A induces aberrant lipid accumulation

An additional phenotype that I observed in HeLa cell lines stably expressing E203G lamin A was the accumulation of lipid droplets (LDs; Fig. 8A and B). To compare size and number of LDs in each cell line, cells were incubated in the absence or presence of oleic acid and LDs were visualized with the 4,4-Difluoro-1,3,5,7,8-Pentamethyl-4-Bora-3a, 4a-Diaza-s-Indacene (BODIPY) dye. In the absence of oleic acid, the diameter of LDs observed in cells stably expressing E203G were approximately two times larger than that in cells carrying an empty vector (Vec) and cells stably expressing WT or K201R. When oleic acid was added to the medium, LDs in cell lines stably expressing E203G were larger than those in other cell lines. I next quantified triacylglycerol (TAG), the major component of LDs. Because the TAG content of cells could not be quantified with high confidence without the addition of oleic acid, the cells were incubated with oleic acid before their TAG content was quantified. The TAG content of the cell line stably expressing E203G was significantly higher than that of the Vec cell line. Conversely, the TAG contents of cell lines stably expressing WT or K201R lamin A tended to be significantly lower than that of the Vec cell line (Fig. 8C).

Long-term expression of E203G lamin A induces premature senescence

The large and flattened cells that appeared upon stable expression of E203G lamin A were morphologically similar to senescent cells. I next examined whether these cells develop premature senescence as a consequence of long-term expression of E203G lamin A. HeLa cells carrying human papilloma viruses E6 and E7 are not appropriate for evaluating cellular senescence (Hall & Alexander, 2003). Therefore, I transduced lentivirus expressing lamin A (WT, K201R, or E203G) into human normal foreskin fibroblasts (HFF) and cloned several HFF lines stably expressing HA-lamin A (Fig. 10B). The obtained cell lines were subjected to senescence-associated β -galactosidase (SA β -gal) staining within 1 month after virus transduction. As shown in Fig. 9, SA β -gal positive cells comprised 26% and 14% of the population expressing E203G lamin A but 2% or 1% of the cells expressing WT, and 1% or 3% of K201R lamin A, respectively. Moreover, the expression levels of p53 and p16, which are typical senescence markers, were increased in multinucleated cells stably expressing E203G lamin A (Fig. 9C). These results clearly show that the expression of E203G lamin A causes cellular senescence *via*

the p53 and/or p16^{INK4a} pathways.

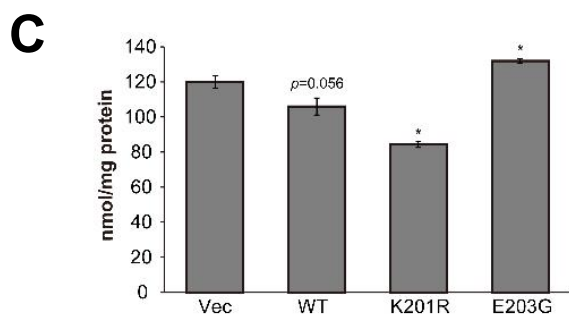
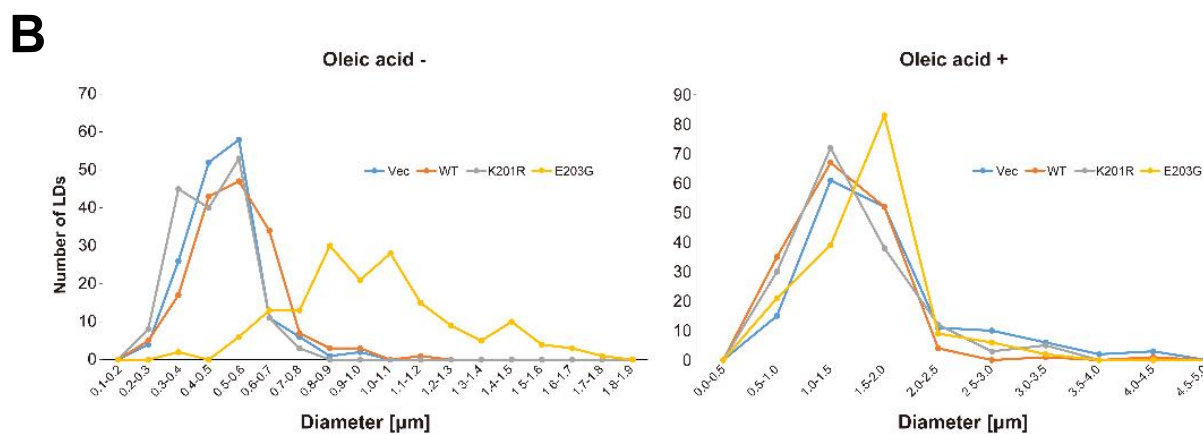
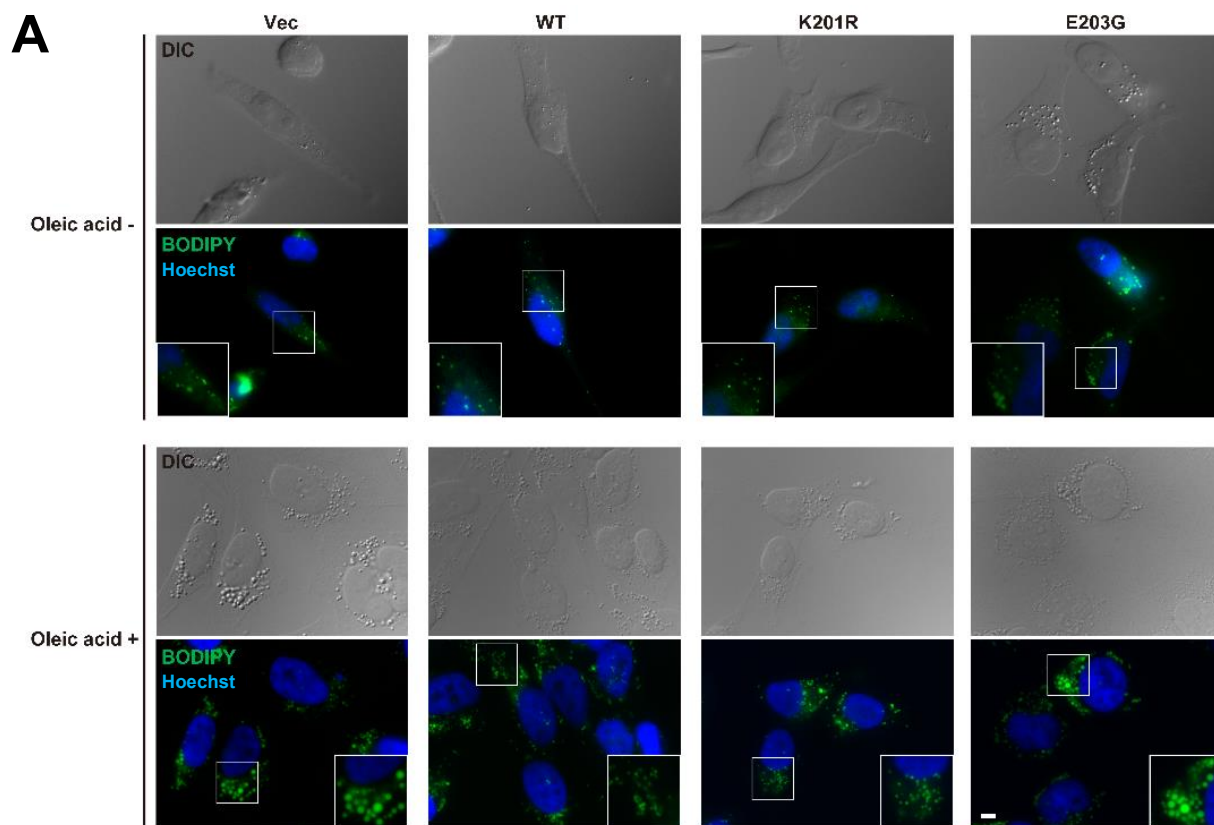


Figure 8. Aberrant lipid accumulation is caused by long-term expression of E203G lamin A. (A) HeLa cells were cultured in the absence or presence of 200 μ M oleic acid for 24h and then HeLa cells fixed and DNA and lipid droplets (LDs) were stained with Hoechst 33258 dye (blue) and bodipy (green), respectively. Bar, 10 μ m. (B) Diameter of 160 LDs in each cell line was measured using Image J and their size distribution and number were shown. (C) Triglyceride contents of each cell lines treated with 200 μ M oleic acid. Data are shown as means \pm SEM. (*, $p < 0.05$ vs. Vec).

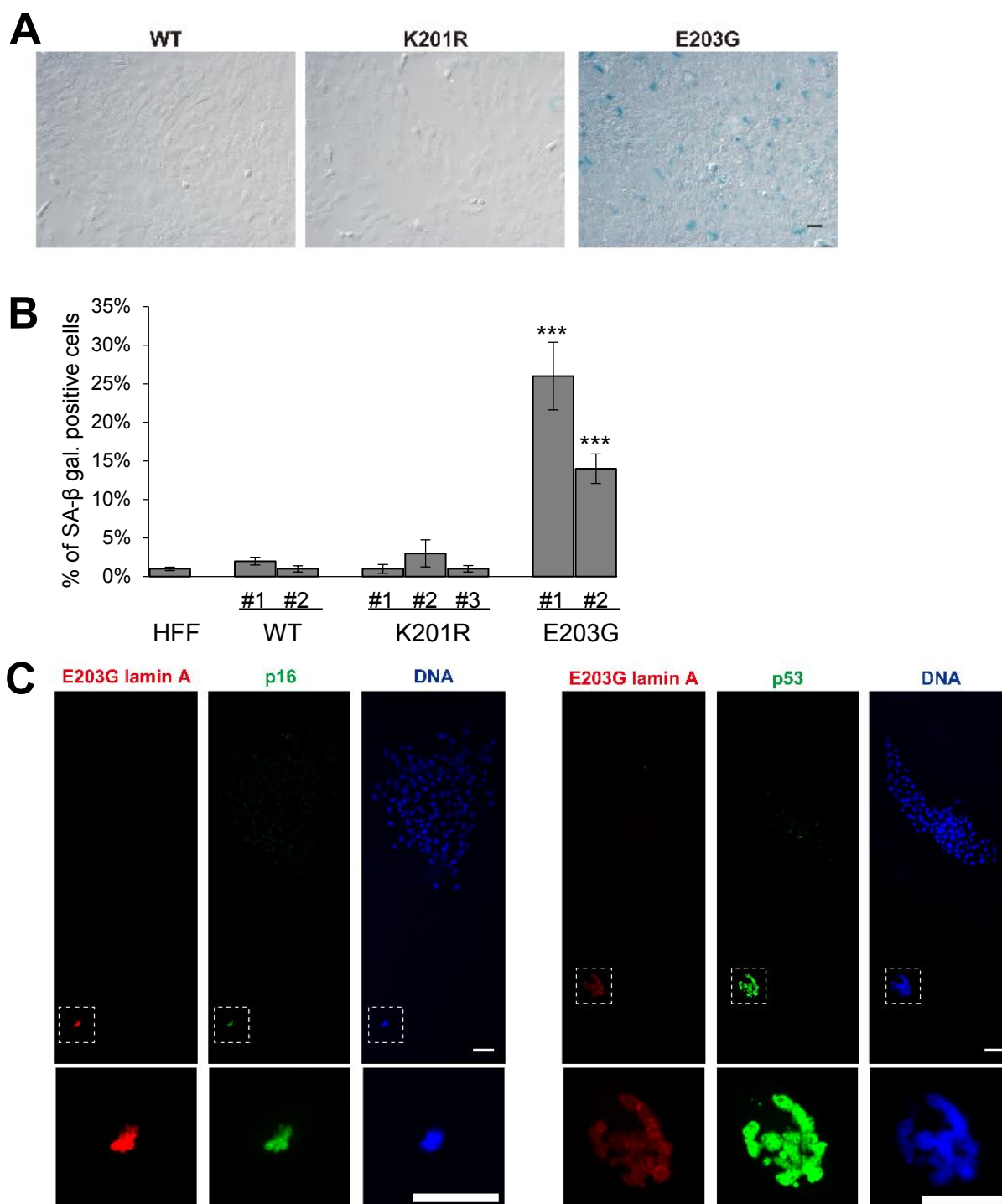


Figure 9. Induction of cellular senescence by long-term expression of E203G lamin A. (A) Immortal HFF cell lines expressing WT, K201R, or E203G lamin A were subjected to SA β -galactosidase staining. Bar, 50 μ m. (B) Quantitative analysis of SA β -Gal-positive cells. Approximately 400–800 cells were scored in eight independent images. Each bar represents data obtained with independent cell lines stably expressing HA-lamin A (WT, K201R, or E203G). Data are shown as means \pm SEM. (***, $p < 0.0005$ vs. WT). (C) Immortal HFF cells were transduced with lentiviruses expressing HA-E203G lamin A. Eleven days after virus transduction, cells were fixed and immunostained with anti-HA antibody (red) and anti-p16^{INK4a} or anti-p53 antibody (green). Typical multinucleated giant cell expressing HA-E203G lamin A is indicated by the dotted square. Bar, 100 μ m.

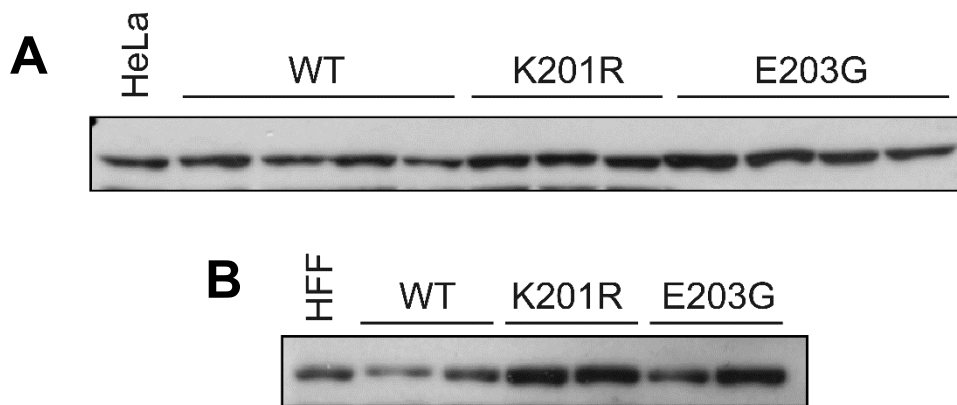


Figure 10. Expression level of HA-lamin A in established cell lines. Expression amounts of HA-lamin A (WT, K201R or E203G) in cell lines established by lentivirus transduction and limiting dilution cloning method were analyzed by western blot using anti-lamin A/C antibody. (A) Parental HeLa cell and cell lines expressing HA-lamin A as indicated. (B) Parental HFF cell and cell lines expressing HA-lamin A as indicated.

2-6. Discussion

In this study, I investigated two lamin A mutations, K201R and E203G, at amino acid residues corresponding to a SUMOylation consensus site. Although these mutations resulted in defective SUMOylation of the lamin A polypeptide, as described in a previous report, K201R and E203G had different properties. For example, a large portion of E203G lamin A was distributed inside the nuclei, whereas K201R lamin A exhibited normal localization. Expression of E203G lamin A diminished the amount of heterochromatin at the nuclear periphery. Assuming that SUMOylation at the K201 residue is important for normal localization and plays a role in heterochromatin formation, expression of the K201R and E203G mutants of lamin A should cause similar phenotypes. Therefore, the varying types of phenotypic disruption caused by the K201R and E203G mutations strongly suggests that loss of SUMOylation is a common feature of these two mutants but may not be a causative defect in cells expressing the E203G mutant. It should be noted that the E203G mutation has been detected in FDC patients, whereas the K201R mutation has not been identified in any laminopathy. These lines of evidence suggest that defective SUMOylation at the K201 position of lamin A is not the predominant cause of FDC. To evaluate the roles of lamin A SUMOylation, I am now screening novel lamin A mutants exhibiting enhanced SUMOylation at K201. I believe that a comparative analysis using a loss of SUMOylation mutant (K201R) and a gain of SUMOylation mutant will provide further insight into SUMOylation of lamin A.

Although the K201R and E203G mutations are located at the center of the N-terminal α -helical rod domain responsible for homodimer formation, an *in vitro* filament formation experiment showed that these mutant lamins retain their capacity for higher-order lamin interactions. I further demonstrated that the K201R and E203G polypeptides could interact with WT lamin in HeLa cells and that E203G lamin A expression clearly disturbs the normal localization of WT lamin A, indicating that E203G expression may interfere with the normal localization or function of WT lamin A in a dominant-negative manner. It is possible that this dominant-negative effect on WT lamin A is involved in the onset of cardiomyopathy induced by the E203G mutation. E203G lamin A did not affect the localization of lamin B1, although E203G lamin A has the capability to interact with lamin B1. Considering that lamin A and lamin B preferentially assemble into homopolymers

comprising either lamin A or lamin B (Delbarre et al., 2006), and that lamin B could be localized to the nuclear membrane by itself via farnesylation on a C-terminal CaaX motif (Dechat et al., 2010), it is conceivable that the E203G mutation does not impair normal lamin B distribution.

Lamin A plays an important role in chromatin organization (Nikolova et al., 2004; Shumaker et al., 2006; Sullivan et al., 1999). In this study, I found that the expression of E203G markedly reduced heterochromatin levels at the nuclear periphery. Because the transcription of many genes is regulated by epigenetic control, it is likely that E203G lamin A disrupts transcriptional regulation through a decline in peripheral heterochromatin levels. Further studies are necessary to elucidate the molecular mechanism of peripheral heterochromatin formation by lamin A.

I observed that lipid accumulation is induced by the long-term expression of the E203G lamin A mutant. Interestingly, fatty metamorphosis has been reported in a member of a family with FDC caused by the E203G mutation (Bharati et al., 1992; Fatkin et al., 1999); however, the nature of the relationship between lipid accumulation and FDC is unknown.

The most striking difference that I observed was the induction of premature senescence. To the best of our knowledge, this is the first report demonstrating that a mutant lamin A associated with cardiomyopathy induces cellular senescence. Some laminopathies have a dominant inheritance pattern, suggesting that the expression levels of the mutant lamin A are nearly equal to those of WT lamin A. Therefore, I adopted a lentivirus carrying the hMTIIA(Δ GRE) promoter expression system to reproduce the appropriate expression balance between the mutant and WT lamin A, and I used this vector to successfully obtain cell lines exhibiting abnormal nuclear morphology and premature senescence. Expression of the typical senescence markers, p53 and p16^{INK4a}, was increased in multinucleated cells stably expressing E203G lamin A. Although it is assumed that the p53 and p16^{INK4a}-pRb pathways are involved in the premature senescence of fibroblasts derived from progeria and lipodystrophy patients (Caron et al., 2007; Kudlow et al., 2008), to the best of my knowledge, this is the first study to demonstrate that mutant lamin A associated with FDC induces senescence via the p53 and p16^{INK4a}-pRb pathways. Although it remains unclear how E203G lamin A induces

cellular senescence, it is possible that the alteration of peripheral heterochromatin levels by E203G lamin A is involved in cellular senescence, as previously reported for progerin (Scaffidi & Misteli, 2005; Shumaker et al., 2006).

In summary, I provide evidence indicating that the expression levels and duration of expression of lamin A mutants are important for understanding the precise mechanisms linking lamin A mutations and abnormal events in nuclei. I believe that long-term expression of mutant lamin A is a simple and appropriate approach for cell biological research on late-onset laminopathies such as dilated cardiomyopathy and lipodystrophy. On the other hand, it is unclear why and how E203G mutant lamin A specifically causes dilated cardiomyopathy. To solve the problem, cardiomyocytes stably expressing E203G mutant lamin A should be established using the expression system used in this study. Cell lines established using available immortalized human cardiomyocytes (for example AC16) (Davidson et al., 2005) and/or ES cells as well as induced pluripotent stem cells (Takahashi & Yamanaka, 2006) might provide a model to understand the relationship between phenotypes and genotypes of laminopathies.

2-7. References

1. Bharati, S., Surawicz, B., Vidaillet, H.J., & Lev, M. (1992). Familial congenital sinus rhythm anomalies: clinical and pathological correlations. *Pacing Clin. Electrophysiol.* **15**, 1720–1729.
2. Bligh, E.G., & Dyer, W.J. (1959). A rapid method of total lipid extraction and purification. *Can. J. Biochem. Physiol.* **37**, 911–917.
3. Broers, J.L. V, Ramaekers, F.C.S., Bonne, G., Yaou, R. Ben, & Hutchison, C.J. (2006). Nuclear lamins: laminopathies and their role in premature ageing. *Physiol. Rev.* **86**, 967–1008.
4. Caron, M., Auclair, M., Donadille, B., Béréziat, V., Guerci, B., Laville, M., Narbonne, H., Bodemer, C., Lascols, O., Capeau, J., & Vigouroux, C. (2007). Human lipodystrophies linked to mutations in A-type lamins and to HIV protease inhibitor therapy are both associated with prelamin A accumulation, oxidative stress and premature cellular senescence. *Cell Death Differ.* **14**, 1759–1767.
5. Davidson, M.M., Nesti, C., Palenzuela, L., Walker, W.F., Hernandez, E., Protas, L., Hirano, M., & Isaac, N.D. (2005). Novel cell lines derived from adult human ventricular cardiomyocytes. *J. Mol. Cell. Cardiol.* **39**, 133–147.
6. Dechat, T., Adam, S.A., Taimen, P., Shimi, T., & Goldman, R.D. (2010). Nuclear lamins. *Cold Spring Harb. Perspect. Biol.* **2**, a000547.
7. Delbarre, E., Tramier, M., Coppey-Moisan, M., Gaillard, C., Courvalin, J.-C., & Buendia, B. (2006). The truncated prelamin A in Hutchinson-Gilford progeria syndrome alters segregation of A-type and B-type lamin homopolymers. *Hum. Mol. Genet.* **15**, 1113–1122.
8. Fatkin, D., MacRae, C., Sasaki, T., Wolff, M.R., Porcu, M., Frenneaux, M., Atherton, J., Vidaillet Jr, H.J., Spudich, S., De Girolami, U., Hospital, B., Clinic, M., & Medical, H. (1999). Missense mutations in the rod domain of the lamin A/C gene as causes of dilated cardiomyopathy and conduction-system disease. *N. Engl. J. Med.* **341**, 1715–1724.
9. Fumoto, T., Yamaguchi, T., Hirose, F., & Osumi, T. (2007). Orphan nuclear

receptor Nur77 accelerates the initial phase of adipocyte differentiation in 3T3-L1 cells by promoting mitotic clonal expansion. *J. Biochem.* **141**, 181–192.

10. Gill, G. (2004). SUMO and ubiquitin in the nucleus: different functions, similar mechanisms? *Genes Dev.* **18**, 2046–2059.
11. Hall, A.H.S., & Alexander, K.A. (2003). RNA interference of human papillomavirus type 18 E6 and E7 induces senescence in HeLa cells. *J. Virol.* **77**, 6066–6069.
12. Hietakangas, V., Ahlskog, J.K., Jakobsson, A.M., Hellesuo, M., Sahlberg, N.M., Holmberg, C.I., Mikhailov, A., Palvimo, J.J., Pirkkala, L., & Sistonen, L. (2003). Phosphorylation of serine 303 is a prerequisite for the stress-inducible SUMO modification of heat shock factor 1. *Mol. Cell. Biol.* **23**, 2953–2968.
13. Kiyono, T., Foster, S.A., Koop, J.I., McDougall, J.K., Galloway, D.A., & Klingelutz, A.J. (1998). Both Rb/p16INK4a inactivation and telomerase activity are required to immortalize human epithelial cells. *Nature* **396**, 84–88.
14. Kotaja, N., Karvonen, U., Jänne, O.A., & Palvimo, J.J. (2002). PIAS proteins modulate transcription factors by functioning as SUMO-1 ligases. *Mol. Cell. Biol.* **22**, 5222–5234.
15. Kudlow, B.A., Stanfel, M.N., Burtner, C.R., Johnston, E.D., & Kennedy, B.K. (2008). Suppression of proliferative defects associated with processing-defective lamin A mutants by hTERT or inactivation of p53. *Mol. Biol. Cell* **19**, 5238–5248.
16. Lloyd, D.J., Trembath, R.C., & Shackleton, S. (2002). A novel interaction between lamin A and SREBP1: implications for partial lipodystrophy and other laminopathies. *Hum. Mol. Genet.* **11**, 769–777.
17. Maraldi, N.M., Capanni, C., Cenni, V., Fini, M., Lattanzi, G., Bavelloni, A., Marmioli, S., & Manzoli, F.A. (2010). Laminopathies and lamin-associated signaling pathways. *Adv. Enzyme Regul.* **50**, 248–261.
18. Nelson, E.J.R., Tuschong, L.M., Hunter, M.J., Bauer, T.R., Burkholder, T.H., & Hickstein, D.D. (2010). Lentiviral vectors incorporating a human elongation factor 1 α promoter for the treatment of canine leukocyte adhesion deficiency. *Gene Ther.* **17**, 672–677.

19. Nikolova, V., Leimena, C., McMahon, A.C., et al. (2004). Defects in nuclear structure and function promote dilated cardiomyopathy in lamin A/C-deficient mice. *J. Clin. Invest.* **113**, 357–369.
20. Sapetschnig, A., Rischitor, G., Braun, H., Doll, A., Schergaut, M., Melchior, F., & Suske, G. (2002). Transcription factor Sp3 is silenced through SUMO modification by PIAS1. *EMBO J.* **21**, 5206–5215.
21. Scaffidi, P., & Misteli, T. (2005). Reversal of the cellular phenotype in the premature aging disease Hutchinson-Gilford progeria syndrome. *Nat. Med.* **11**, 440–445.
22. Schreiber, K.H., & Kennedy, B.K. (2013). When lamins go bad: nuclear structure and disease. *Cell* **152**, 1365–1375.
23. Shumaker, D.K., Dechat, T., Kohlmaier, A., Adam, S. a, Bozovsky, M.R., Erdos, M.R., Eriksson, M., Goldman, A.E., Khuon, S., Collins, F.S., Jenuwein, T., & Goldman, R.D. (2006). Mutant nuclear lamin A leads to progressive alterations of epigenetic control in premature aging. *Proc. Natl. Acad. Sci. U. S. A.* **103**, 8703–8708.
24. Solovei, I., Wang, A.S., Thanisch, K., et al. (2013). LBR and lamin A/C sequentially tether peripheral heterochromatin and inversely regulate differentiation. *Cell* **152**, 584–598.
25. Stuurman, N., Heins, S., & Aebi, U. (1998). Nuclear lamins: their structure, assembly, and interactions. *J. Struct. Biol.* **122**, 42–66.
26. Subramanian, L., Benson, M.D., & Iñiguez-Lluhí, J. a (2003). A synergy control motif within the attenuator domain of CCAAT/enhancer-binding protein alpha inhibits transcriptional synergy through its PIASy-enhanced modification by SUMO-1 or SUMO-3. *J. Biol. Chem.* **278**, 9134–9141.
27. Sullivan, T., Escalante-Alcalde, D., Bhatt, H., Anver, M., Bhat, N., Nagashima, K., Stewart, C.L., & Burke, B. (1999). Loss of A-type lamin expression compromises nuclear envelope integrity leading to muscular dystrophy. *J. Cell Biol.* **147**, 913–920.
28. Takahashi, K., & Yamanaka, S. (2006). Induction of pluripotent stem cells from

- mouse embryonic and adult fibroblast cultures by defined factors. *Cell* **126**, 663–676.
29. Weber, K., Plessmann, U., & Traub, P. (1989). Maturation of nuclear lamin A involves a specific carboxy-terminal trimming, which removes the polyisoprenylation site from the precursor; implications for the structure of the nuclear lamina. *FEBS Lett.* **257**, 411–414.
 30. Yamashita, D., Yamaguchi, T., Shimizu, M., Nakata, N., Hirose, F., & Osumi, T. (2004). The transactivating function of peroxisome proliferator-activated receptor γ is negatively regulated by SUMO conjugation in the amino-terminal domain. *Genes to Cells*, doi: 10.1111/j.1365-2443.2004.00786.x.
 31. Yamashita, D., Komori, H., Higuchi, Y., Yamaguchi, T., Osumi, T., & Hirose, F. (2007). Human DNA replication-related element binding factor (hDREF) self-association via hATC domain is necessary for its nuclear accumulation and DNA binding. *J. Biol. Chem.* **282**, 7563–7575.
 32. Ye, Q., & Worman, H.J. (1995). Protein-protein interactions between human nuclear lamins expressed in yeast. *Exp. Cell Res.* **219**, 292–298.
 33. Ye, Z.-Q., Qiu, P., Burkholder, J.K., Turner, J., Culp, J., Roberts, T., Shahidi, N.T., & Yang, N.-S. (1998). Cytokine transgene expression and promoter usage in primary CD34⁺ cells using particle-mediated gene delivery. *Hum. Gene Ther.* **9**, 2197–2205.
 34. Zhang, Y.-Q., & Sarge, K.D. (2008). Sumoylation regulates lamin A function and is lost in lamin A mutants associated with familial cardiomyopathies. *J. Cell Biol.* **182**, 35–39.

3. Functional analysis of lamin A SIM: Requirement of lamin A SIM for lamin A reassembly at the end of mitosis

3-1. Summary

Modification of proteins with small ubiquitin-related modifier (SUMO; SUMOylation) is involved in the regulation of various biological processes. Recent studies have demonstrated that noncovalent associations between SUMOylated proteins and cooperative proteins containing SUMO-interacting motifs (SIMs) are important for the spatiotemporal organization of many protein complexes. In this study, I demonstrate that interactions between lamin A, a major component of the nuclear lamina, and SUMO isoforms are dependent on one of the four SIMs (SIM3) resided in lamin A polypeptide in vitro. Live cell imaging and immunofluorescence staining showed that SIM3 is required for accumulation of lamin A on the chromosomes during telophase, and subsequent evaluation of a panel of deletion mutants determined that a 156-amino acid region spanning the carboxyl-terminal Ig-fold domain of lamin A is sufficient for this accumulation. Notably, mutation of SIM3 abrogated the dephosphorylation of mitosis-specific phosphorylation at Ser-22 of lamin A, which normally occurs during telophase, and the subsequent nuclear lamina reorganization. Furthermore, expression of a conjugation-defective SUMO2 mutant, which was previously shown to inhibit endogenous SUMOylation in a dominant-negative manner, also impaired the accumulation of wild type lamin A on telophase chromosomes. These findings suggest that interactions between SIM3 of lamin A and a putative SUMO2-modified protein plays an important role in the reorganization of the nuclear lamina at the end of mitosis.

3-2. Abbreviations

NPC, the nuclear pore complex; SIM, SUMO-interacting motif; BAF, barrier-to-autointegration factor; AKAP149, A-kinase-anchoring protein 149; GST, glutathione S-transferase; PP1, protein phosphatase 1; NLS, nuclear localization signal

3-3. Introduction

The nuclear lamina is a fibrous structure located beneath the inner nuclear membrane that interacts with chromatin, the nuclear pore complex (NPC), and LEM (LAP2, emerin, MAN1)-domain proteins, which are integral proteins that localize to the inner membrane of the nuclear envelope, thereby contributing both to nuclear structural stability and to regulation of chromatin organization in higher eukaryotes (Andrés and González, 2009). The lamina is composed primarily of two types of lamins: A-type (lamin A/C) and B-type (lamin B1, B2) lamins. Lamin polypeptides have well-defined conserved domains, including an N-terminal head domain, a central α -helical rod domain, and a C-terminal tail domain (Parry et al., 1986), and both types of lamins are known to self-assemble into higher-order structures through multiple steps. First, the lamin polypeptides form a coiled-coil dimer through parallel association of two α -helical rod domains. Next, the lamin dimers associate in a head-to-tail fashion. Finally, intermediate filaments are formed by the interaction of these polymers in an antiparallel fashion (Dechat et al., 2010). During mammalian cell mitosis, the nuclear lamina, as well as the NPC and LEM-domain proteins, is disassembled and reassembled. Notably, however, both the timing of nuclear lamina disassembly and the pathways governing reassembly differ between A-type and B-type lamins (Georgatos et al., 1997; Moir et al., 2000). For instance, A-type lamins exhibit barrier-to-autointegration factor (BAF)-dependent localization to a specialized region of the telophase chromosome mass near the spindle, termed the “core” region, and organize the nuclear lamina while interacting with BAF and the LEM-domain protein emerin. In contrast, B-type lamins and NPC components accumulate at the non-core regions of telophase chromosomes (Haraguchi et al., 2008).

It is assumed that phosphorylation plays a key role in the regulation of lamin disassembly/assembly. Phosphorylation of lamins occurs at specific sites within the head and tail domains, and is mediated by mitotic kinases or cyclin-dependent kinase 1 (Cdk1) both in vivo and in vitro (Peter et al., 1990; Hocevar et al., 1993; Goss et al., 1994). Notably, the phosphorylation of lamin A at the beginning of mitosis acts as a trigger for nuclear envelope breakdown (Ward and Kirschner, 1990; Heald and McKeon, 1990). Meanwhile, dephosphorylation of lamins by protein phosphatase 1 (PP1) is required for nuclear lamina reassembly during telophase and early G1 (Thompson et al., 1997). Lamin

B has also been reported to be dephosphorylated by the PP1/A-kinase-anchoring protein 149 (AKAP149) complex (Steen et al., 2000), and Steen and Collas (2001) demonstrated that inhibition of AKAP149 binding by PP1 results in abrogated assembly of B-type lamins. The location(s) at which A-type lamins are dephosphorylated during telophase, however, and the mechanism by which this process is regulated have yet to be elucidated. Recent studies demonstrated that post-translational modification of proteins with small ubiquitin-related modifier (SUMO; SUMOylation) plays essential roles in both mitotic progression and phosphorylation. Indeed, immunostaining and biochemical analyses of mitotic cells indicated that SUMO1 and SUMO2/3 are conjugated to distinct proteins during mitosis. While SUMO1-modified proteins localize to the mitotic spindle during early mitosis and to the spindle midzone during late mitosis, SUMO2/3-modified proteins localize to the centromeres and kinetochores during prophase and metaphase, and appear to coat the chromosome arms at the metaphase-anaphase transition (Zhang et al., 2008). In particular, modification with SUMO2/3 results in localization of topoisomerase II to centromeres, while SUMO2/3-modified Nuf2 and BubR1 were found to recruit CENP-E to kinetochores (Azuma et al., 2005; Agostinho et al., 2008; Zhang et al., 2008). However, the precise function of the SUMO2/3-modified proteins that coat the chromosomes remains unclear.

SUMOylation of proteins can mediate novel protein-protein interactions with other proteins containing SUMO-interacting motifs (SIMs). The SIM is a hydrophobic motif with a loose consensus sequence (V/L/I-X-V/L/I-V/L/I) that interacts non-covalently with the hydrophobic groove of SUMO (Song et al., 2004; Hecker et al., 2006; Minty et al., 2000) and is involved in protein complex formation and the spatiotemporal tethering of SUMOylated proteins to specific structures such as the PML (promyelocytic leukemia) nuclear body, kinetochores, and transcription machinery (Lin et al., 2006; Zhang et al., 2008; Gómez-del Arco et al., 2005). Although a number of SUMOylated proteins have been identified, and various effects of SUMOylation on these proteins have been partially characterized, the significance of such SUMO-SIM interactions is largely unclear.

In this study, I identified four potential SUMO-interacting motifs (SIMs) within the lamin A polypeptide and generated a panel of SIM-defective lamin A mutants to investigate the function of these motifs. Our findings demonstrate that a SIM located within the carboxyl-

terminal Ig-fold domain of lamin A, referred to hereafter as SIM3, is required for the chromosomal accumulation of lamin A during telophase. Furthermore, I show that SIM3 plays an integral role in the proper dephosphorylation of mitosis-specific phosphorylation of lamin A during telophase, and in subsequent nuclear lamina reorganization. I propose that the activity of this SIM during the later stages of mitosis may be mediated by a SUMO2-modified protein(s) that is associated with telophase chromosomes.

3-4. Experimental procedures

Plasmids

The plasmids used for mammalian expression of HA-tagged WT and lamin A SIM mutants were generated by inserting the respective human lamin A cDNA molecules into the pCSII-hMTIIA(Δ GRE)-HA-IRES2-Venus lentivirus vector containing the human metallothionein-IIA promoter, as described previously (Moriuchi et al., 2014). Meanwhile, 6 \times His- and GFP-tagged lamin A WT and SIM mutants were generated by inserting lamin A coding sequences between the *Bam*HI and *Eco*RI restriction sites of the pET47b vector (Merck Millipore), and between the *Eco*RI and *Bam*HI restriction sites of the previously constructed CSII-MT-GFP vector (Hashimoto et al., 2012), respectively. Base substitution mutations were introduced into the lamin A cDNA *via* site-specific mutagenesis using the overlap extension method, and were confirmed by DNA sequencing. While the WT SUMO1 and SUMO2 constructs were generated as described previously (Yamashita et al., 2004), the lamin A SIM mutants, lamin A deletion mutants, SUMO2 (G93A) mutant were generated by PCR using the following primers:

Lamin A SIM1(EE), Forward: 5'-GACCCGAGAGGAGGAGATTGACAATGGGA-3'

Reverse: 5'-AATCTCCTCCTCTCGGGTCTCATGACGGC-3'

SIM2(EE), Forward: 5'-CCAGGAGGAAGAGGACATCAAGCTGGCCCT-3'

Reverse: 5'-GATGTCCTCTTCCTCCTGGTACTCGTCCAG-3'

SIM3(EE), Forward: 5'-GCTGGGCAGGAGGAGACGATCTGGGCTGC-3'

Reverse: 5'-CCA GATCGTCTCCTCCTGCCAGCCTTCA-3'

SIM4(EE), Forward: 5'-TCAGTGACTGAGGAAGAGGACGACGAGGAT-3'

Reverse: 5'-CGTCGTCCTCTTCCTCAGTCACTGAGCGCA-3'

1-383, Forward: 5'-GGAGAATTCAGAGACCCCGTCCCAGCGGCG-3'

Reverse: 5'-GAGGATCCTCACTCGCCCTCCAAGAGCTTGCGGTA-3'

384-664, Forward: 5'-CCAGAATTCGGAGGAGAGGCTACGCCTGT-3'

Reverse: 5'-GAAGGATCCTTACATGATGCTGCAGTTCTG-3'

417-664, Forward: 5'-TTAGAATTCGAAAAGCGCAAAGTGGAGT-3'

Reverse: 5'-GAAGGATCCTTACATGATGCTGCAGTTCTG-3'

436-664, Forward: 5'-TTAGAATTCGACTAGCGGGCGCGTGGCC-3'

Reverse: 5'-GAAGGATCCTTACATGATGCTGCAGTTCTG-3'

384-572, Forward: 5'-CCAGAATTCGGAGGAGAGGCTACGCCTGT-3'

Reverse: 5'-AATGGATCCTTAGCTGCTGCAGTGGGAGCCG-3'

384-544, Forward: 5'-CCAGAATTCGGAGGAGAGGCTACGCCTGT-3'

Reverse: 5'- ATGGATCCTTACACCAGCTTGCGCATGGCCACTTC-3'

417-572, Forward: 5'-TTAGAATTCGAAAAAGCGCAAACCTGGAGT-3'

Reverse: 5'-AATGGATCCTTAGCTGCTGCAGTGGGAGCCG-3'

SUMO2 (G93A), Forward: 5'-GTAAGATCTATGCCGACGAAAAGCCCAAGG-3'

Reverse: 5'-GTAGTCGACTCAGTAGACAGCTCCCGTCT-3'

Cell culture and DNA transfection

HeLa cells were cultured in Ham's F-12 medium containing 10% fetal bovine serum (FBS; Nichirei Bioscience) at 37°C under 5% CO₂. 293FT cells were maintained in DMEM (high glucose) supplemented with 10% FBS, 0.1 mM non-essential amino acids (Gibco [Invitrogen]), 100 U/ml penicillin, 1 µg/ml streptomycin, 29.2 µg/ml L-glutamine, and 100 µg/ml G418 (Promega) at 37°C under 5% CO₂.

Transfection of plasmid DNA into HeLa cells was performed using the calcium phosphate method for immunofluorescence and the Polyethylenimine "Max" (Mw 4,000) (Polysciences) method for synchronizing experiments. For the calcium phosphate method, 1×10^5 cells were seeded in 12-well plates and cultured overnight. The following day, DNA/calcium phosphate precipitates containing 3 µg of the indicated expression plasmids were added to each well. After 4 h, the precipitates were removed, and cells were cultured for 24 h in the appropriate medium. For polyethylenimine (PEI) transfection, DNA/PEI complexes containing 4 µg of HA-lamin A (WT or SIM3[EE]) and 12 µg of PEI were added to cells cultured in 60-mm cell culture dishes.

Antibodies

The mouse anti-human lamin A/C monoclonal antibodies (clone 636; 1:2000 and 1:500 dilution for Western blotting [WB] and Immunofluorescence staining [IF], respectively), the mouse anti-c-myc monoclonal antibodies (clone 9E10; 1:500 dilution) and the rabbit anti-cyclin B1 polyclonal antibodies (1:5000 dilution) were purchased from Santa Cruz Biotechnology, the rat anti-HA monoclonal antibodies (clone 3F10; 1:500 dilution) and the mouse anti-His monoclonal antibodies (clone His-2; 1:5000 dilution) were purchased from Roche, the mouse anti-FLAG monoclonal antibodies (clone M2; 1:5000 and 1:500

dilution for WB and IF, respectively) were obtained from Sigma-Aldrich. The rabbit anti-phospho-lamin A/C (Ser22) monoclonal antibodies (clone D2B2E; 1:2000 and 1:2500 dilution for WB and IF, respectively) were purchased from Cell Signaling Technology. Meanwhile, horseradish peroxidase-conjugated secondary antibodies specific to rat, mouse, and rabbit immunoglobulin G (IgG; NA935, NA9310, and NA934V, respectively, 1:7000 dilution) were obtained from GE Healthcare Life Sciences. Anti-rat and anti-mouse species-specific antibodies conjugated to Alexa Fluor 594 (A-11007 and A-11005) and Alexa Fluor 488 (A-11006 and A-11001) were purchased from Life Technologies. All Alexa Fluor-conjugated antibodies were used at a 1:500 dilution.

Western blotting

PVDF membranes were blocked by incubation with 5% skim milk in Tris-buffered saline (TBS) for 30 minutes, and then probed by incubation with the indicated primary antibodies diluted in TBS containing 0.05% Tween-20 (TBST) and 5% skim milk at 4°C overnight, followed by the appropriate HRP-conjugated secondary antibodies suspended in TBST. Bands were detected using an enhanced chemiluminescence (ECL) western blotting detection kit (Thermo Scientific).

Immunofluorescence and fluorescence microscopy

Cells were grown on glass coverslips, washed with PBS, fixed by incubating in 2% paraformaldehyde in PBS for 20 min, permeabilized in PBS containing 0.3% Triton X-100 for 15 min, and blocked with 2% BSA in PBS. The coverslips were then incubated overnight with the appropriate primary antibodies diluted in PBS containing 0.1% BSA at 4°C. After three washes with PBS, the coverslips were incubated for 1 h with Alexa Fluor 488- or Alexa Fluor 594-conjugated secondary antibodies in PBS containing 0.1% BSA at 4°C. DNA was stained with Hoechst 33258 dye (Calbiochem). After two washes with PBS, the coverslips were mounted on glass slides spotted with ProLong Gold and SlowFade Gold antifade reagents (Life Technologies).

For live cell imaging experiments, cells were grown in glass-bottom culture dishes (Iwaki), transfected with GFP(105)-fusion plasmids, and placed in a stage-top incubator (Tokai Hit) for approximately 22–30 h. GFP(105) is a GFP mutant that contains the S65T/F64L/V163A/S175G amino acid substitutions that exhibits enhanced fluorescence intensity (Yamasaki et al., 1998). The fluorescent immunocomplexes and GFP(105)-

tagged proteins were imaged using an oil-immersion objective lens (PLAPO 63×/NA 1.4) and a Leica HyD detector mounted on a Leica TCS SP8 confocal laser scanning immunofluorescence microscope (Leica Microsystems). Image processing was performed using Adobe Photoshop software.

Quantitative colocalization analysis of immunofluorescence confocal images

The Fiji program was used to quantify the degree of colocalization between the two indicated fluorescence signals. Prophase, anaphase and telophase cells were selected, and the entire cellular region of each selected cell was examined. Pearson's correlation coefficient was calculated using the Fiji plug-in colocalization threshold program.

GST pull-down assay

His-tagged recombinant WT lamin A and SIM mutants were expressed in *Escherichia coli* cells and extracted with lysis buffer (20 mM Tris-HCl [pH 8.0], 150 mM NaCl, 0.5% Triton X-100) containing 6 M urea. His-tagged lamin A proteins were then precipitated by incubation with glutathione-sepharose beads covered with GST-SUMO-1, -2, or -3 in lysis buffer containing 2 M urea. GST and GST-SUMO polypeptides were eluted from the beads in 5 mM reduced glutathione, separated by SDS-PAGE, and detected by immunoblotting using anti-His antibodies. GST and GST-SUMOs were also detected by Coomassie brilliant blue staining after separation by SDS-PAGE.

Cell synchronization

HeLa cells were synchronized in mitosis using thymidine, hydroxyurea, and nocodazole blocks. The cells were presynchronized in S phase by incubation with 2.0 mM thymidine for 20 h, transfected at 6 h after release from thymidine, and further incubated for 7 h at 37°C. The cells were resynchronized at the G1/S transition by incubation with 1.5 mM hydroxyurea for 13 h. The G1/S cells were then washed, incubated in fresh medium for 11 h, and synchronized at the early phase of mitosis by treatment with medium containing 100 ng/ml nocodazole for 6 h. Mitotic cells were collected by the shake-off method, aliquoted, and cultured in fresh nocodazole-free medium for the indicated lengths of time. The cells were then immediately lysed in sample buffer.

Statistical analysis

Student's t test was utilized to evaluate statistically significant differences between results. $p < 0.05$ was considered statistically significant.

3-5. Results

Identification of a SIM that is necessary for the interaction of lamin A with SUMO *in vitro*

Four regions matching the consensus SIM amino acid sequence were identified in lamin A using the GPS-SUMO (Zhao et al., 2014) with the low threshold (Fig. 1A). To evaluate the interaction between lamin A and SUMO, I first performed a GST pull-down assay using a recombinant 3×His tagged lamin A and the three GST-SUMO isoforms, respectively. While His-lamin A was pulled down by GST-SUMO1, -SUMO2, and -SUMO3, but not by GST (Fig. 1B), the intensity of the lamin A bands from the GST-SUMO2 and -SUMO3 pull-downs were notably greater than that from the GST-SUMO1 pull-down sample. This result suggests that lamin A directly interacts with all isoforms of SUMO, but that the interactions between lamin A and SUMO2 and SUMO3 seem to be stronger than that with SUMO1 *in vitro*. To determine which of the four SIM consensus sequences is necessary for the interaction between lamin A and SUMO2 *in vitro*, I examined the SUMO-binding abilities of a series of SIM-defective lamin A mutants (SIM[EE]) that were generated by substituting two hydrophobic amino acids with glutamic acid residues within each respective SIM (Fig. 1C) (Lin et al., 2006). His-tagged WT lamin A, as well as His-tagged lamin A proteins carrying single, double, or triple EE mutations in SIM1, SIM2, and/or SIM4, were effectively pulled down by GST-SUMO2. Conversely, the His-lamin A protein carrying the SIM3(EE) mutation was not pulled down by GST-SUMO2. These results suggest that SIM3 is necessary and sufficient for the interaction between lamin A and SUMO2 *in vitro*.

SIM3 is responsible for the association of lamin A with telophase chromosomes

To examine the role of the four SIMs in the subcellular localization of lamin A, the HA-tagged WT lamin A and SIM(EE) mutants were transiently expressed in HeLa cells and visualized by immunofluorescence staining (Fig. 2A). At 24 h post-transfection, each of the four SIM(EE) mutants exhibited lamina localization patterns that were similar to that of the WT. Furthermore, there were no obvious differences in the signal intensities between the SIM(EE) mutants and WT lamin A. Surprisingly, however, at 48 h after transfection, the cells expressing SIM2(EE) and SIM3(EE) displayed abnormal nuclear laminas with small and spherical foci, respectively. These abnormalities emerged after

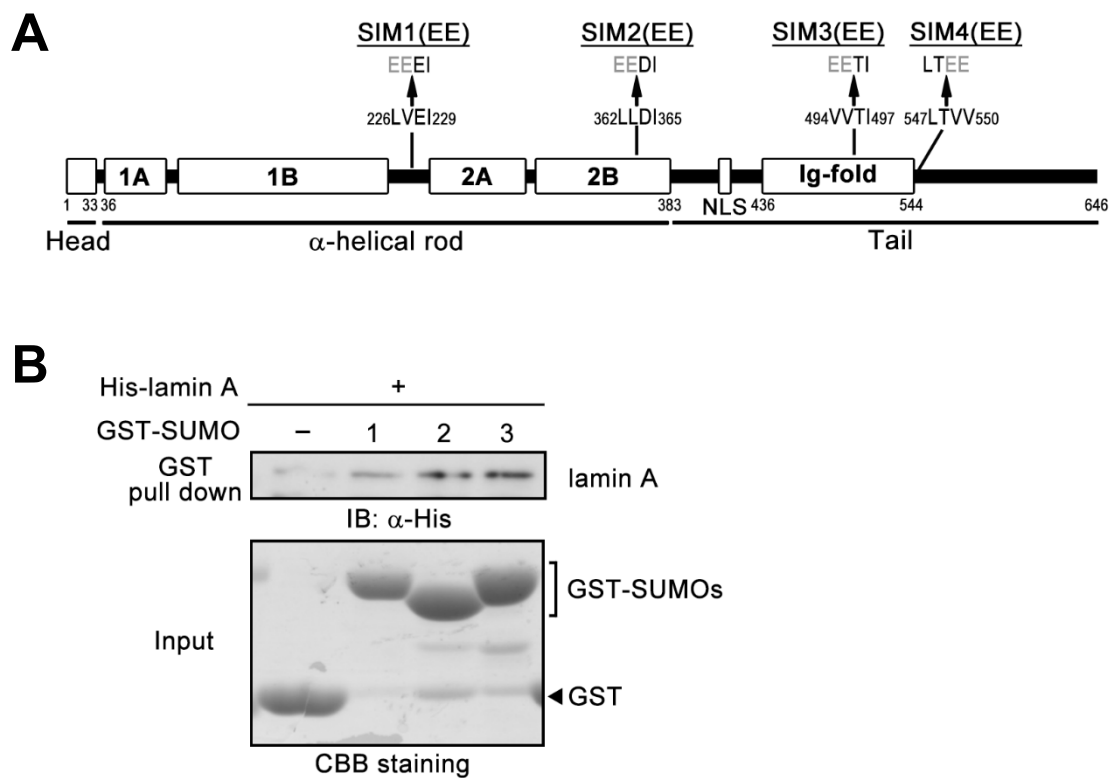


Fig. 1. Identification of SUMO-interacting motifs (SIMs) in lamin A. (A) Domain structure of the lamin A polypeptide. SIM(EE) mutants were generated by substitution of two hydrophobic amino acids with glutamic acid residues in each respective SIM. (B) Interaction between lamin A and small ubiquitin-related modifier 1 (SUMO1), 2, and 3. A lysate prepared from an *Escherichia coli* culture expressing His-lamin A was added to glutathione-sepharose beads that were preadsorbed with GST, GST-SUMO1, GST-SUMO2, or GST-SUMO3. After incubation and extensive washing, the proteins were eluted with 5 mM reduced glutathione and separated by sodium dodecyl sulfate polyacrylamide gel electrophoresis (SDS-PAGE). His-lamin A was then detected by western blot analysis using an anti-His antibody. Meanwhile, GST and the GST-SUMO paralogs were visualized by Coomassie brilliant blue staining (CBB). The data is representative of two independent experiments with similar results.

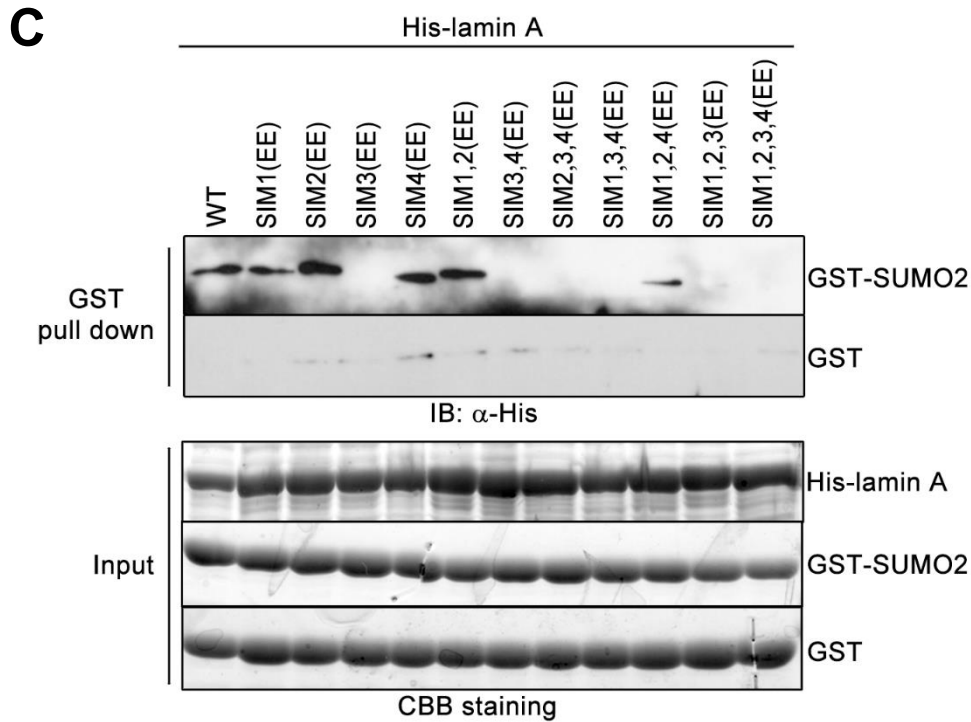


Fig. 1. Identification of SUMO-interacting motifs (SIMs) in lamin A.

(C) Analysis of interactions between SUMO2 and lamin A SIM(EE) mutants *in vitro*. Wild type (WT) lamin A and a series of His-lamin A mutant proteins were expressed in *E. coli* and subjected to GST pull-down analysis, as described in (B). His-lamin A proteins were pulled down using glutathione-sepharose beads preadsorbed with either GST or GST-SUMO2, and detected by western blot analysis with an anti-His antibody. The data is representative of two independent experiments with similar results. His-lamin A, GST, and GST-SUMO2 were visualized by Coomassie staining.

cell division, raising the possibility that mutation of these SIMs might impair the disassembly or assembly of lamin A during mitosis. Therefore, to monitor the dynamics of lamin A during mitosis in living cells, I generated a panel of fluorescent lamin A reporters (Fig. 2B). Both SIM2(EЕ) and SIM3(EЕ) exhibited normal disassembly at the beginning of mitosis, and there were no significant differences in the localization patterns of the GFP-fused WT and SIM mutants between prophase and metaphase (data not shown). However, the two mutants exhibited abnormal localization at the later stage of mitosis. GFP-fused WT lamin A began to associate with the mitotic chromosomes at 7 min after the metaphase-anaphase transition (indicated as time 0), where it accumulated at the core region, and the nuclear lamina was organized after at least 17 min, as previously reported (Haraguchi et al., 2008). Meanwhile, GFP-SIM2(EЕ) exhibited a fluorescence pattern similar to that of WT lamin A; however, small foci were observed after 17 min surrounding the daughter nuclei. Conversely, GFP-SIM3(EЕ) did not localize to mitotic chromosomes at 7 min and exhibited low levels of accumulation at the core regions. Instead, small foci of SIM3(EЕ) appeared in non-core regions at 9–11 min, the period during which WT lamin A accumulated at the core region. Furthermore, the SIM3(EЕ) mutant formed a number of small foci and appeared to be enriched at the proximal non-core regions of the telophase chromosomes.

Next, I transiently expressed HA-tagged wild type and SIM3(EЕ) lamin A in HeLa cells and examined the subcellular distributions of these proteins during cell cycle progression. Consistent with the results obtained using the GFP-labeled reporters, the distribution patterns of SIM3(EЕ) lamin A in interphase cells and in mitotic cells at prophase, prometaphase, metaphase, and anaphase were similar to those of wild type HA-lamin A, as well as to those of endogenous lamina A (data not shown). Notably, however, the SIM3(EЕ) mutant exhibited abnormal localization in cells at telophase. As shown in Fig. 2C, while endogenous lamin A/C and the transiently expressed HA-WT lamin A accumulated on telophase chromosomes and at the peripheral region of chromosomes, the SIM3(EЕ) mutant was not detected on the mitotic chromosomes and did not assemble into nuclear lamina at the peripheral region of chromosomes during telophase. These results suggest that SIM3 is required for the accumulation of lamin A on telophase chromosomes and for the reassembly of lamin A. To validate this hypothesis,

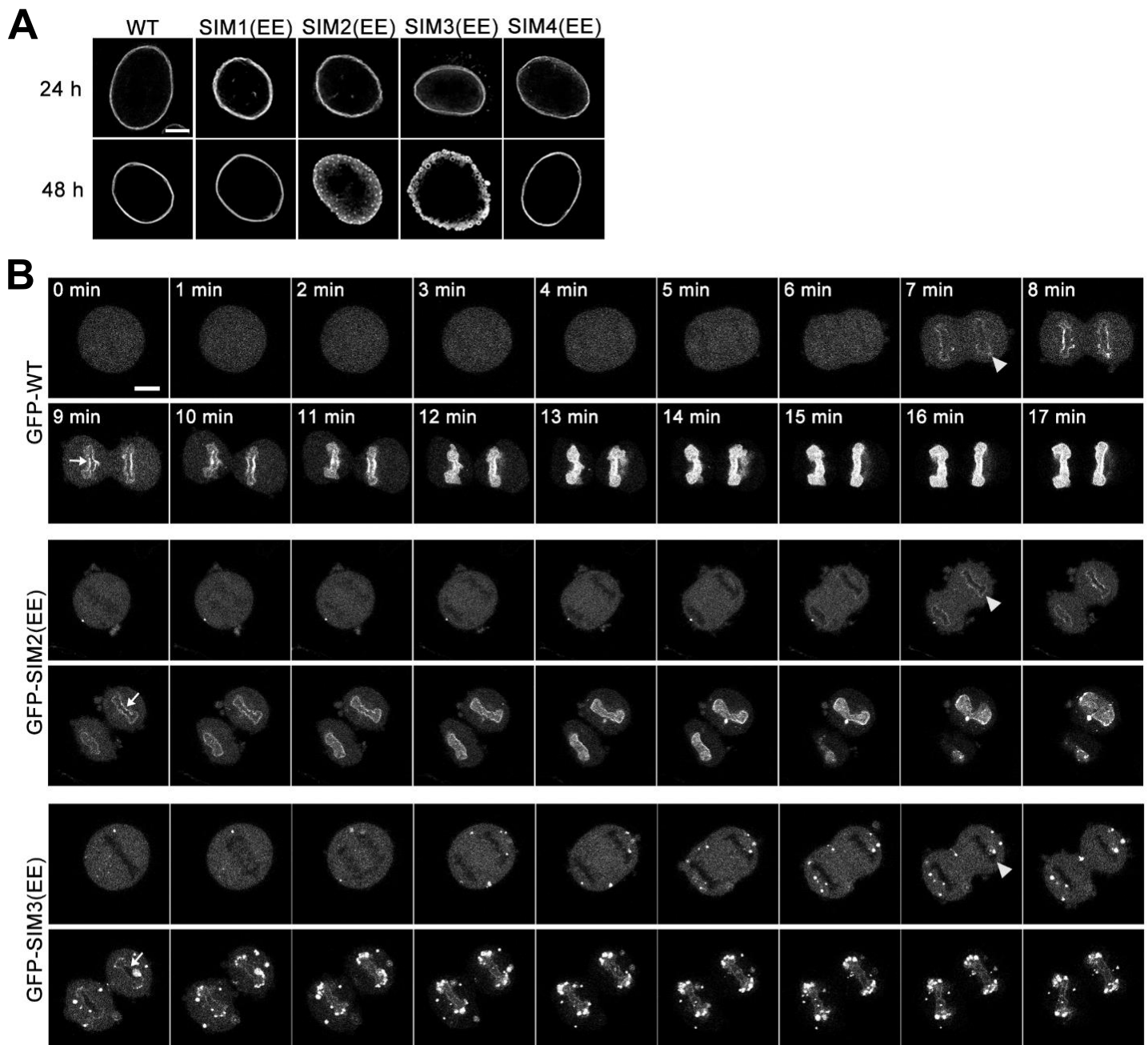


Fig. 2. Abnormal localization of the lamin A SUMO-interacting motif 3 (SIM3) mutant protein during mitosis. (A) HeLa cells were transfected with plasmids expressing HA-tagged lamin A proteins [wild type (WT), SIM1(EЕ), SIM2(EЕ), SIM3(EЕ), or SIM4(EЕ)], and visualized by confocal immunofluorescence microscopy at 24 h or 48 h after transfection. Bar, 5 μ m. The images are representative of cells examined in three independent experiments (24 h, $n > 5$; 48 h, $n > 20$). (B) HeLa cells were transfected with plasmids expressing GFP-tagged WT, SIM2(EЕ), or SIM3(EЕ) and cultured for 22–30 h. Live images of cells were captured at 1-min intervals until the end of cytokinesis using confocal microscopy. The time-lapse images obtained are shown from left to right, with time point 0 indicating the metaphase-anaphase transition. Bar, 10 μ m. Note that WT lamin A and the SIM2(EЕ) mutant, but not the SIM3(EЕ) mutant, associated with telophase chromosomes at 7 min (indicated by arrows), and accumulated at the “core” region at 9 min (indicated by arrowheads). The images are representative of cells examined in at least two independent experiments ($n > 3$).

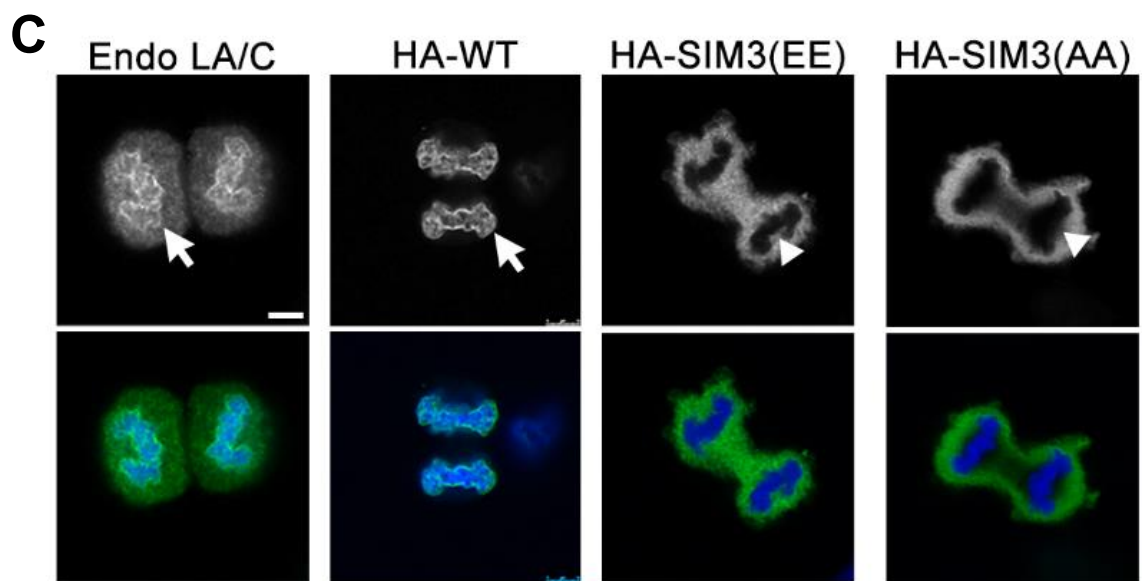


Fig. 2. Abnormal localization of the lamin A SUMO-interacting motif 3 (SIM3) mutant protein during mitosis. (C) Non-transfected HeLa cells and cells transfected with plasmids expressing HA-lamin A [WT, SIM3(EE) or SIM3(AA)] proteins were subjected to immunofluorescence staining using anti-lamin A/C or anti-HA antibodies (green) at 24 h post-transfection. DNA was stained with Hoechst 33258 dye (blue). Bar, 5 μ m. Note that endogenous lamin A/C and HA-WT lamin A localized to telophase chromosomes (indicated by arrows), while the SIM3(EE) and (AA) mutant did not (indicated by arrowhead). The images are representative of cells examined in three independent experiments ($n > 3$).

I created an additional SIM3 mutant in which two hydrophobic valine residues within the domain were substituted with alanine residues (SIM3[AA]), and examined the subcellular localization of this protein during telophase. Similar to SIM3(EE), SIM3(AA) did not accumulate on telophase chromosomes, supporting the requirement of SIM3 for accumulation of lamin A on telophase chromosomes. It should be noted that expression of the SIM3(EE) mutant did not prominently disturb the organization of the nuclear envelope, as determined by immunostaining of endogenous emerin, lamin B, RanBP2, and Nup153 during cytokinesis; however, the nuclear envelope exhibited an abnormal structure during the late G1 phase (Fig. 3). Moreover, the majority of cells transiently expressing SIM3(EE) ceased proliferating after only a few cycles of cell division (Fig. 4). Therefore, I speculate that SIM3 may be required for normal reorganization of the nuclear envelope.

Next, I utilized a set of GFP-fused lamin A deletion mutants to characterize the amino acid region that is sufficient for chromosomal targeting of lamin A during telophase (Fig. 5A). Interestingly, the region comprising amino acids 417–572, which contains the C-terminal Ig-fold domain and nuclear localization signal (NLS), was itself capable of effectively accumulating on telophase chromosomes (Fig. 5B), indicating that dimer formation through the α -helical rod domain at the N-terminus may be dispensable for lamin A accumulation on telophase chromosomes. Consistent with these findings, deletion of residues 417–572 (lamin A^{417–572/SIM3(EE)}) abolished lamin A accumulation on the telophase chromosomes (Fig. 5C). Therefore, I concluded that the C-terminal 156 amino acids are responsible for mediating lamin A accumulation on telophase chromosomes, and that SIM3 is crucial for this process.

SIM3 plays an important role in the dephosphorylation of lamin A during telophase

As described above, lamin A SIM3(EE) failed to accumulate on telophase chromosomes and to form a normal nuclear lamina. Because it was previously shown that phosphorylation and dephosphorylation of lamin A, particularly at Ser-22 (S22) and Ser-392 (S392), are required for nuclear lamina disassembly and reassembly during mitosis, respectively (Heald and McKeon, 1990), I investigated the effects of the SIM3(EE) mutation on lamin A phosphorylation and dephosphorylation during mitosis. Fluctuations in the phosphorylation and localization of endogenous lamin A/C and HA-lamin A (WT

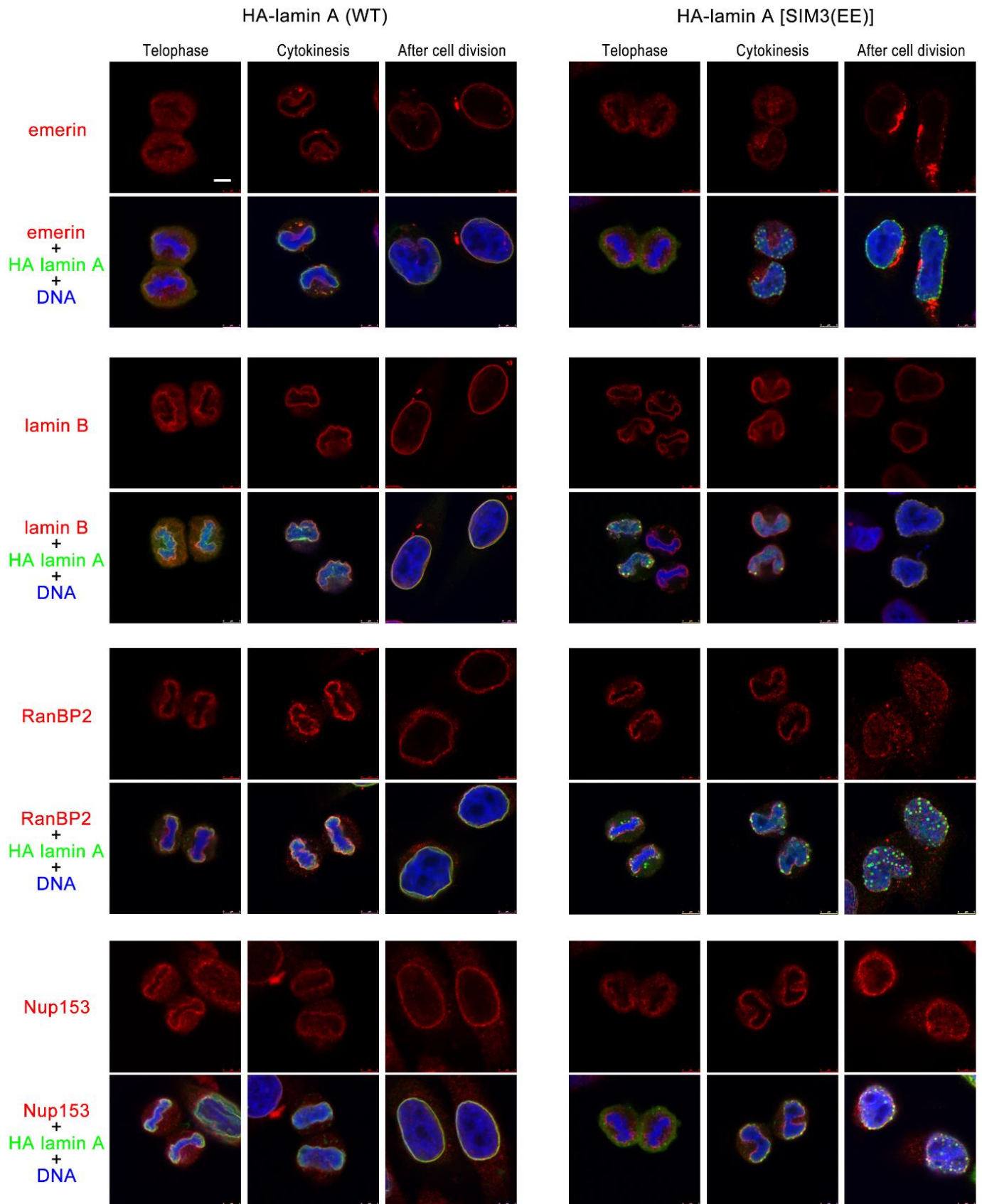


Fig. 3. The effects of a lamin A SUMO-interacting motif 3 (SIM3) mutant on the intracellular localization of emerin, lamin B1, RanBP2, and Nup153. HeLa cells were transfected with plasmids expressing HA-tagged wild type (WT) lamin A or lamin A SIM3(EE). At 28 h after transfection, the cells were fixed and stained with an anti-HA antibody (green), and with anti-emerin, anti-lamin B1, anti-RanBP2, or anti-Nup153 antibodies (red). DNA was stained with Hoechst 33258 dye (blue). Confocal images of each phase of mitosis are shown ($n > 3$ for each mitosis stage). Bar, 5 μ m.

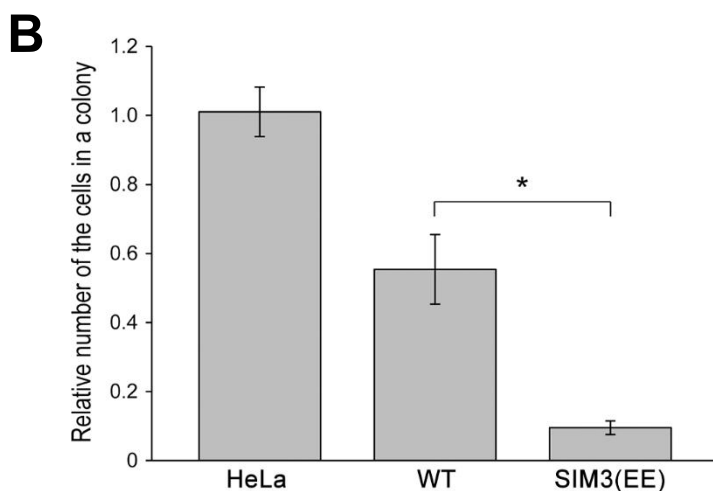
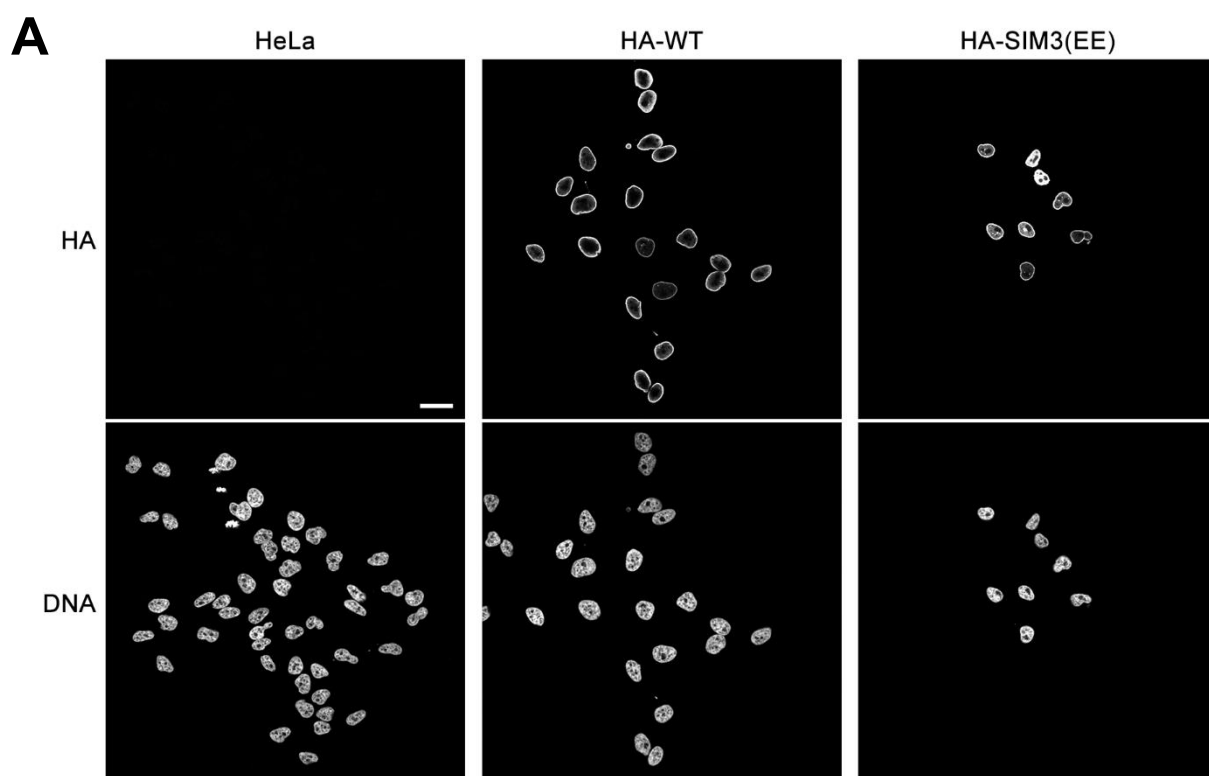


Fig. 4. The effects of a lamin A SUMO-interacting motif 3 (SIM3) mutant on cell proliferation. (A) Untreated HeLa cells and cells transfected with plasmids expressing HA-tagged wild type (WT) lamin A or lamin A SIM3(EE) were fixed and stained with anti-HA, anti-phosphorylated lamin A/C (Ser22) antibodies, and Alexa Fluor 594- and 488-conjugated secondary antibodies, respectively, at 72 h post-transfection. DNA was stained with Hoechst 33258 dye (blue). Bar, 25 μ m. (B) The numbers of cells expressing HA-lamin A relative to the number of non-transfected cells are included in the graph. Three colonies of non-transfected cells and five colonies of transfected cells were measured. Data are shown as means \pm standard errors of the mean (SEM). * p < 0.05 vs. WT.

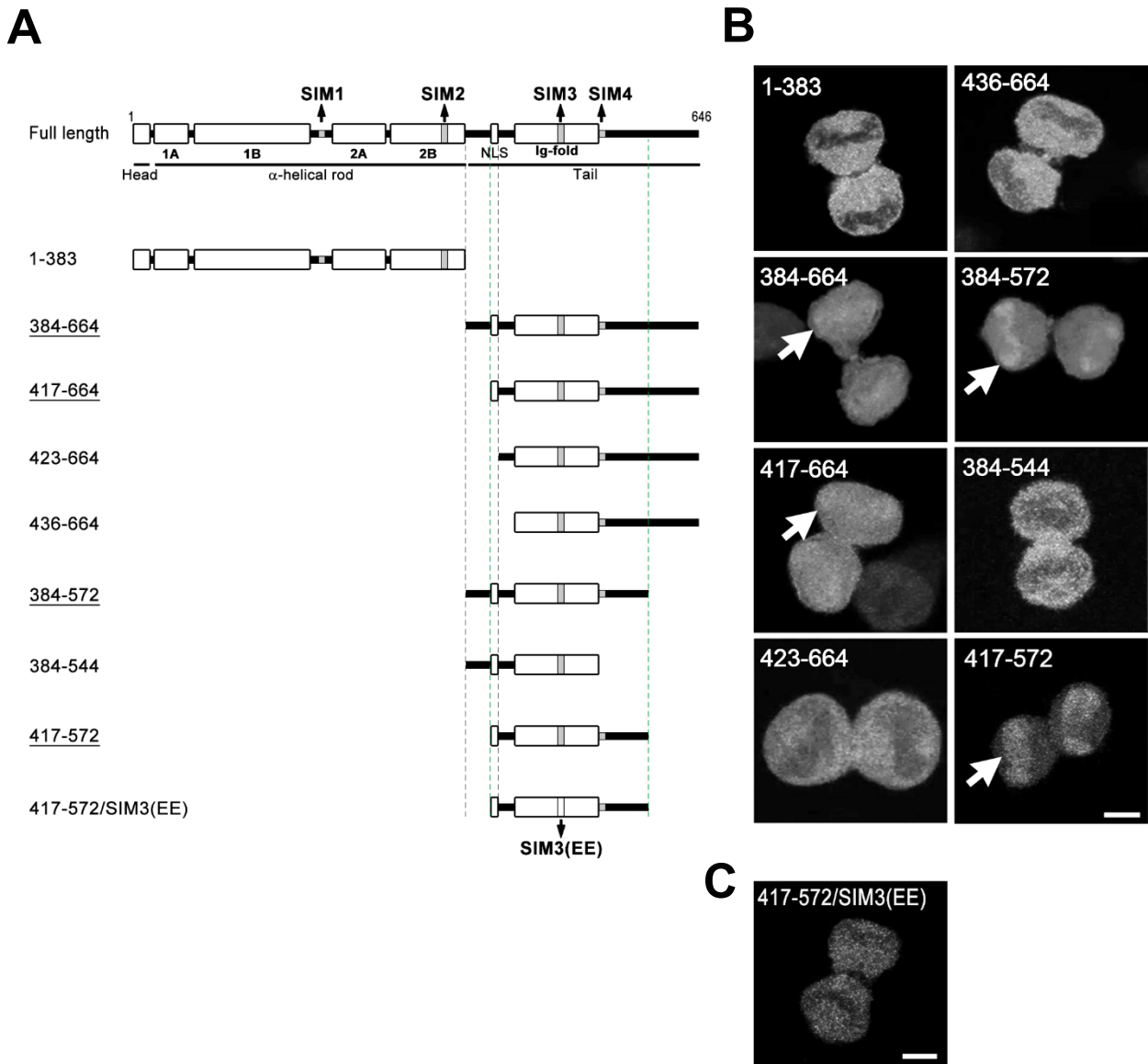


Fig. 5. Accumulation of lamin A deletion mutants on telophase chromosomes. (A) Schematic domain structure of the lamin A deletion mutants. Underline indicates that the deletion mutants exhibited accumulation on telophase chromosomes. Green colored dashed lines indicate the region responsible for accumulation on telophase chromosomes. (B and C) HeLa cells were transfected with plasmids expressing GFP-fused lamin A deletion mutant (B) or lamin A^{417-572/SIM3(EE)} mutant (C), and fixed at 27 h after transfection. The images were obtained by confocal fluorescence microscopy. The 384-664, 417-664, 384-572, and 417-572 deletion mutants (indicated by arrows), but not the 1-383, 423-664, 436-664, 384-544 and 417-572/SIM3(EE) deletion mutants, exhibited chromosomal localization during telophase. Bar, 5 μ m. The images are representative of cells examined in three independent experiments (n > 3).

and SIM3[EE]) during mitosis were monitored by immunofluorescence staining using an antibody specific for lamin A/C phosphorylated at serine 22 (pS22) (Fig. 6A). For detailed observation, I divided telophase into two definitive phases (telophase I and telophase II) based on chromosomal morphology and the presence or absence of prenucleolar bodies (Savino et al., 2001; Carron et al., 2012), as depicted in Fig. 7. There was no difference in lamin A pS22 localization between non-transfected cells and cells expressing HA-WT lamin A. Lamin A pS22 signals appeared in the nucleoplasm concurrently with the beginning of prophase, and were dispersed in the cytoplasm until entry into telophase. Notably, pS22 signals promptly accumulated on chromosomes in telophase I, and then decreased as telophase progressed. Meanwhile, the subcellular localization pattern of pS22 in HeLa cells expressing the SIM3(EE) mutant were quite similar to those in HeLa cells with or without HA-WT lamin A during prophase, prometaphase, metaphase, and anaphase. However, the accumulation of pS22 on telophase chromosomes was not observed in cells expressing SIM3(EE). Moreover, highly intense pS22 signals remained throughout the latter phase of telophase (telophase II) and cytokinesis (Fig. 4A), and SIM3(EE) expression resulted in markedly increased numbers of p22-positive interphase cells at 72 h after transfection (Fig. 6D). These results suggest that, in addition to its role in promoting the accumulation of lamin A on telophase chromosomes, SIM3 is required for proper dephosphorylation of lamin A at the end of mitosis.

Because lamin A dephosphorylation during late mitosis seemed to be inhibited by expression of the SIM3(EE) mutant, I next quantified changes in the levels of lamin A pS22 during mitosis by immunoblot analysis. For these analyses, HeLa cells were transfected with plasmids expressing HA-tagged WT lamin A or SIM3(EE) and synchronized at the beginning of mitosis, according to the protocol illustrated in Fig. 4B. Cells were collected by shaking, transferred to fresh medium, harvested, and lysed at various time points. Synchronization and cell cycle progression were evident by fluctuations in cyclin B1 expression levels (Fig. 6C). Dephosphorylation of HA-WT lamin A was clearly observed at 1.5 h after release from the nocodazole block. In contrast, I detected scarce amounts of dephosphorylation of lamin A in cells expressing SIM3(EE) at 1.5 h after the release from mitotic arrest, and the relative amount of pS22 in cells expressing SIM3(EE) was approximately four-fold higher than that in cells expressing

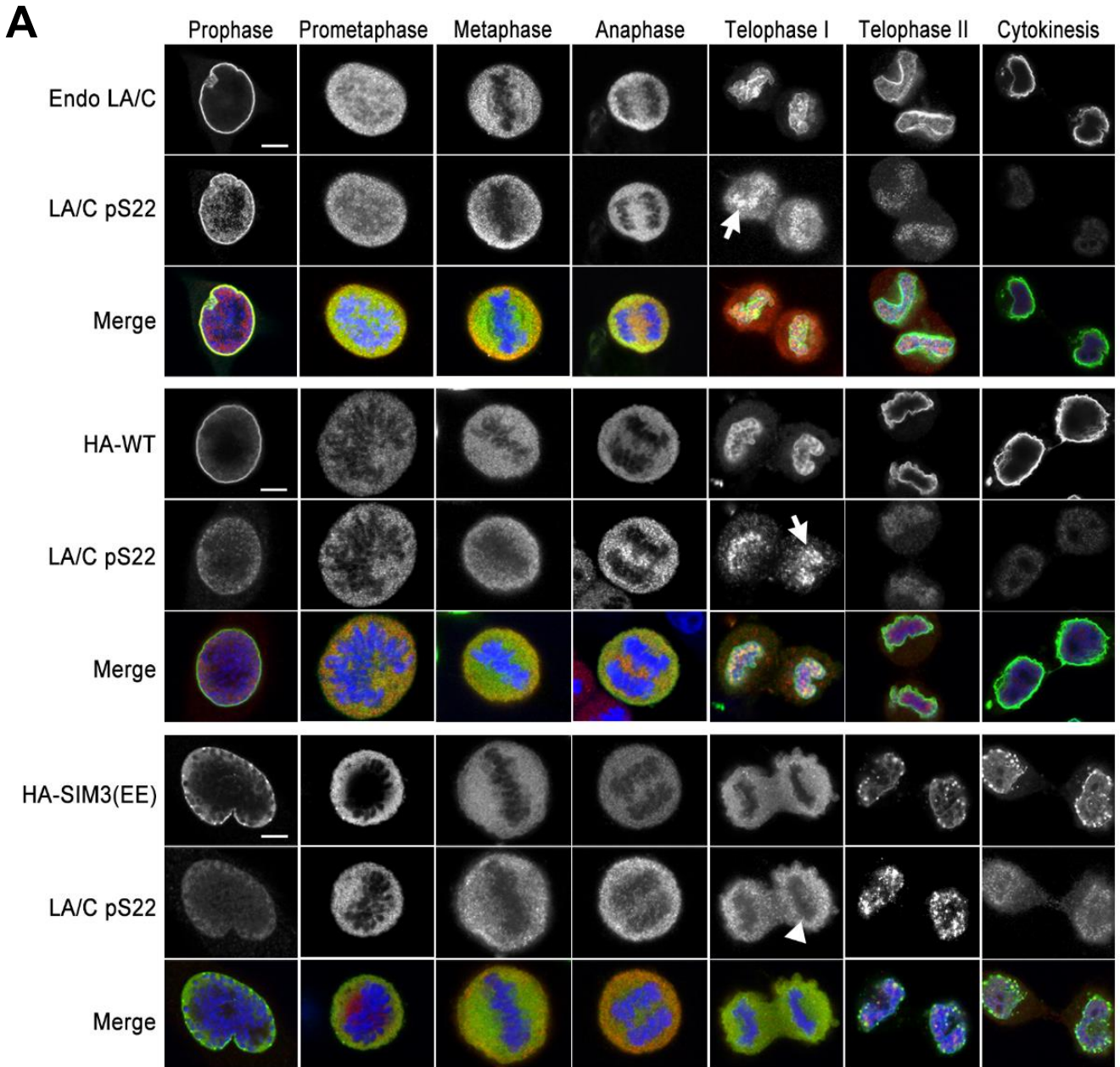


Fig. 6. Effect of the SUMO-interacting motif 3 (SIM3) (EE) mutation on the phosphorylation/dephosphorylation of lamin A. (A) Upper panel: HeLa cells were stained using anti-lamin A/C (endo LA/C; green) and anti-phosphorylated lamin A/C (Ser22) (LA/C pS22; red) antibodies. Middle and lower panels: HeLa cells were transfected with plasmids expressing HA-tagged wild type (WT) lamin A or lamin A SIM3(EE). At 28 h after transfection, the cells were fixed and stained using anti-HA (green) and anti-LA/C pS22 (red) antibodies. DNA was stained with Hoechst 33258 dye (blue). Confocal images of each phase of mitosis are shown. Bar, 5 μ m. Note that lamin A/C pS22 accumulated on telophase chromosomes in non-transfected cells and in cells expressing HA-WT lamin A (indicated by arrow), but not in 86.6% of fifteen cells expressing HA-lamin A SIM3(EE) (indicated by arrowhead).

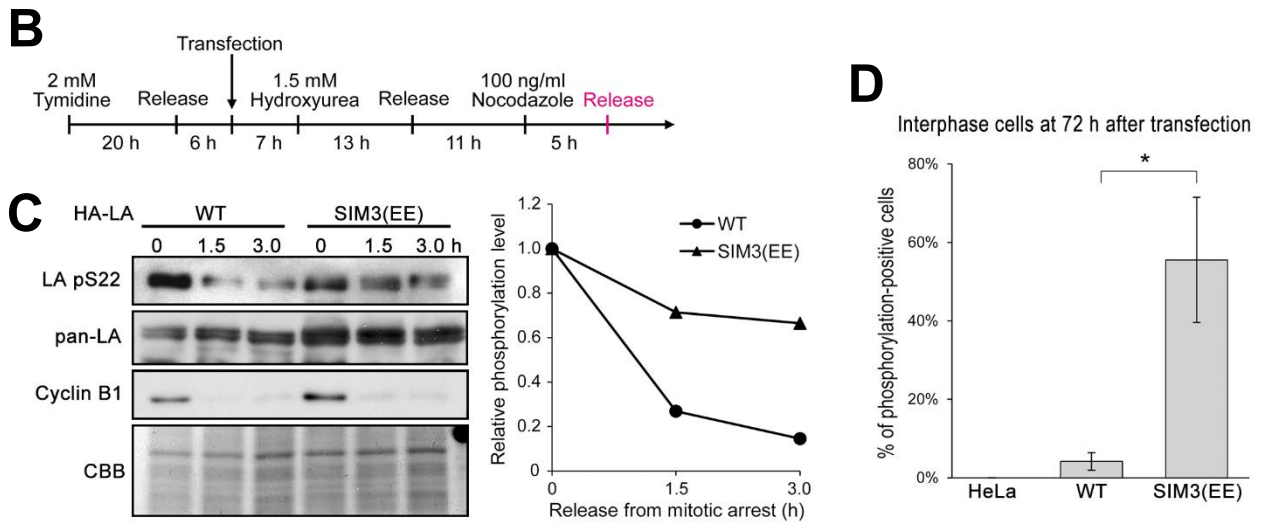
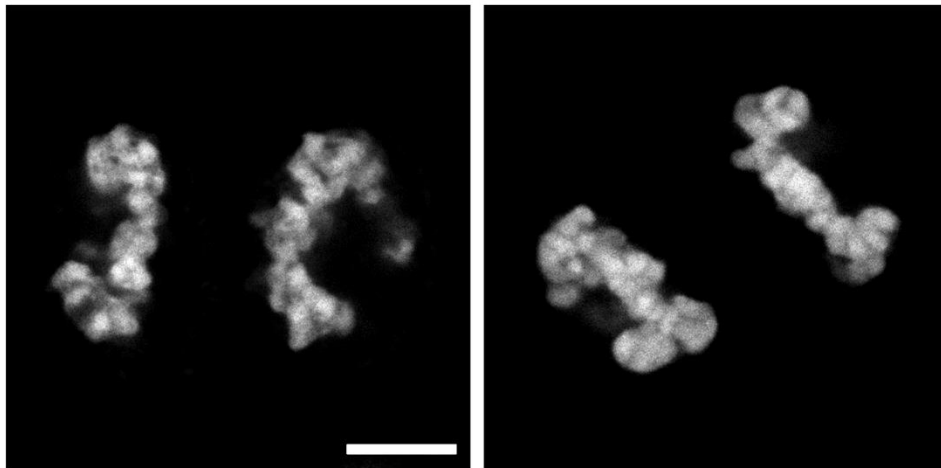


Fig. 6. Effect of the SUMO-interacting motif 3 (SIM3) (EE) mutation on the phosphorylation/dephosphorylation of lamin A. (B) Schematic depiction of the synchronization method. (C) HeLa cells transiently expressing HA-WT lamin A or HA-lamin A SIM3(EE) were synchronized in mitosis, as described in B. Cells were then collected and directly lysed in Laemmli sample buffer at the indicated time points after release from the blockage. The samples were then subjected to sodium dodecyl sulfate polyacrylamide gel electrophoresis (SDS-PAGE) and proteins were detected by western blot analysis using anti-LA/C pS22, pan-lamin A/C (pan-LA) and anti-cyclin B1 antibodies. The graph on the right summarizes the results of the quantification of phosphorylated lamin A band signals. The values denote the ratio of the phosphorylation signal intensity normalized to the Coomassie brilliant blue (CBB)-stained proteins at each time point, compared to that in the 0 h sample. The data is representative of two independent experiments with similar results. (D) The percentages of the number of LA/C pS22-positive cells during interphase are shown in the graph. Non-transfected HeLa cells and cells transfected with plasmids expressing HA-wild type (WT) lamin A or SIM3(EE) were fixed at 72 h post-transfection and stained with anti-HA and anti-LA/C pS22 antibodies, and Alexa Fluor 594 and 488-conjugated secondary antibodies, respectively. Non-transfected or transfected cells were analyzed using ImageJ software (HeLa; n = 102, WT; n = 58, SIM3(EE); n = 36). Quantification of phosphorylation-positive cells number was performed using the ImageJ threshold/analyze particle features (threshold: 30–255). Data are shown as means \pm standard errors of the mean (SEM). * $p < 0.05$ vs. WT.

Telophase I



Telophase II

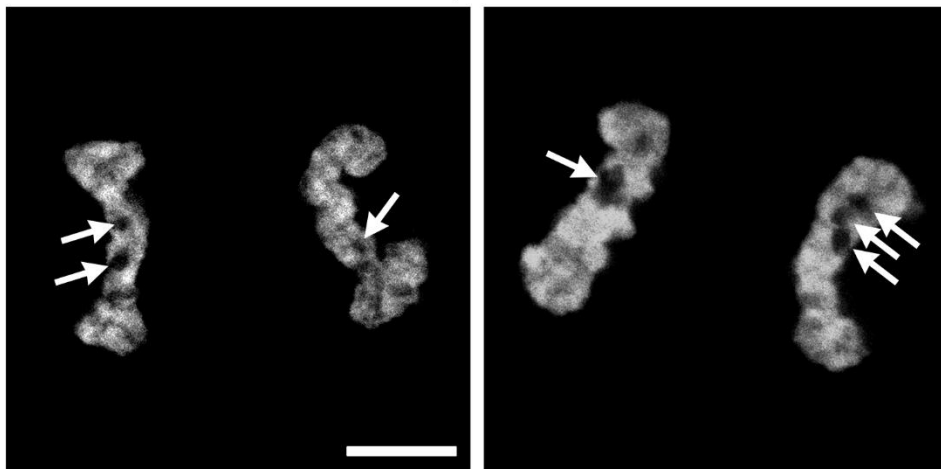


Fig. 7. Representative images of telophase I and telophase II. During telophase I, the chromosome arms, but not the pre-nucleolar body or nucleolus, are visible. In telophase II, the chromosome arms disappear and pre-nucleolar bodies (arrows), which are known to appear at the end of telophase, are visible. Bar, 5 μ m.

WT lamin A at 3.0 h. Again, these findings demonstrate the significance of SIM3 for proper lamin A dephosphorylation at the end of mitosis.

Expression of a conjugation-defective SUMO2 mutant inhibits the localization of lamin A to telophase chromosomes

Given the significance of SIM3 for proper lamin A dynamics during the later phase of mitosis, I speculated that SIM-mediated interactions between unknown SUMOylated protein(s) and lamin A would be involved in lamin A accumulation on telophase chromosomes. To explore this possibility, I first examined whether endogenous SUMO1 and SUMO2/3 colocalized with lamin A on telophase chromosomes. As shown in Fig. 8A and C, while SUMO1 partially localized to the region surrounding the telophase chromosomes, it did not colocalize with lamin A/C on the chromosomes during this period. In contrast, SUMO2/3 began to accumulate on the chromosomes in telophase I (Fig. 8B). Since lamin A pS22 also accumulated on chromosomes during telophase I (Fig. 6A), I measured the levels of colocalization between lamin A/C pS22 and SUMO2/3 by quantitative colocalization analysis of confocal immunofluorescence images using Fiji software (Fig. 8C and D). Although colocalization signals (white color signals) were scarcely detected in cells during prophase or anaphase, significant levels of partial colocalization were detected in cells during telophase I (Fig. 8C and D).

To obtain further evidence for the participation of SUMOylated protein(s) in lamin A accumulation on telophase chromosomes, I generated an expression plasmid encoding the SUMO2 (G93A) mutant, which cannot covalently bind to target proteins, and has been shown to inhibit endogenous SUMOylation in a dominant-negative manner (Li et al., 2003; Schou et al., 2014). I examined the effects of G93A expression on the localization pattern of WT lamin A in telophase I by simultaneously expressing HA-WT lamin A and myc-SUMO2 (WT or G93A) in HeLa cells (Fig. 9A). Surprisingly, while abundant myc-SUMO1 (WT) was detected on telophase chromosomes, only scant chromosomal localization of myc-SUMO2 (G93A) was observed. Given that G93A is incapable of conjugating to target proteins, the myc-SUMO2 (WT) signals on telophase chromosomes may correspond to protein(s) conjugated to myc-SUMO2. Expression of G93A, but not WT SUMO2, impaired the accumulation of WT lamin A on telophase chromosomes as well as the reassembly of lamin A at peripheral chromosomal regions.

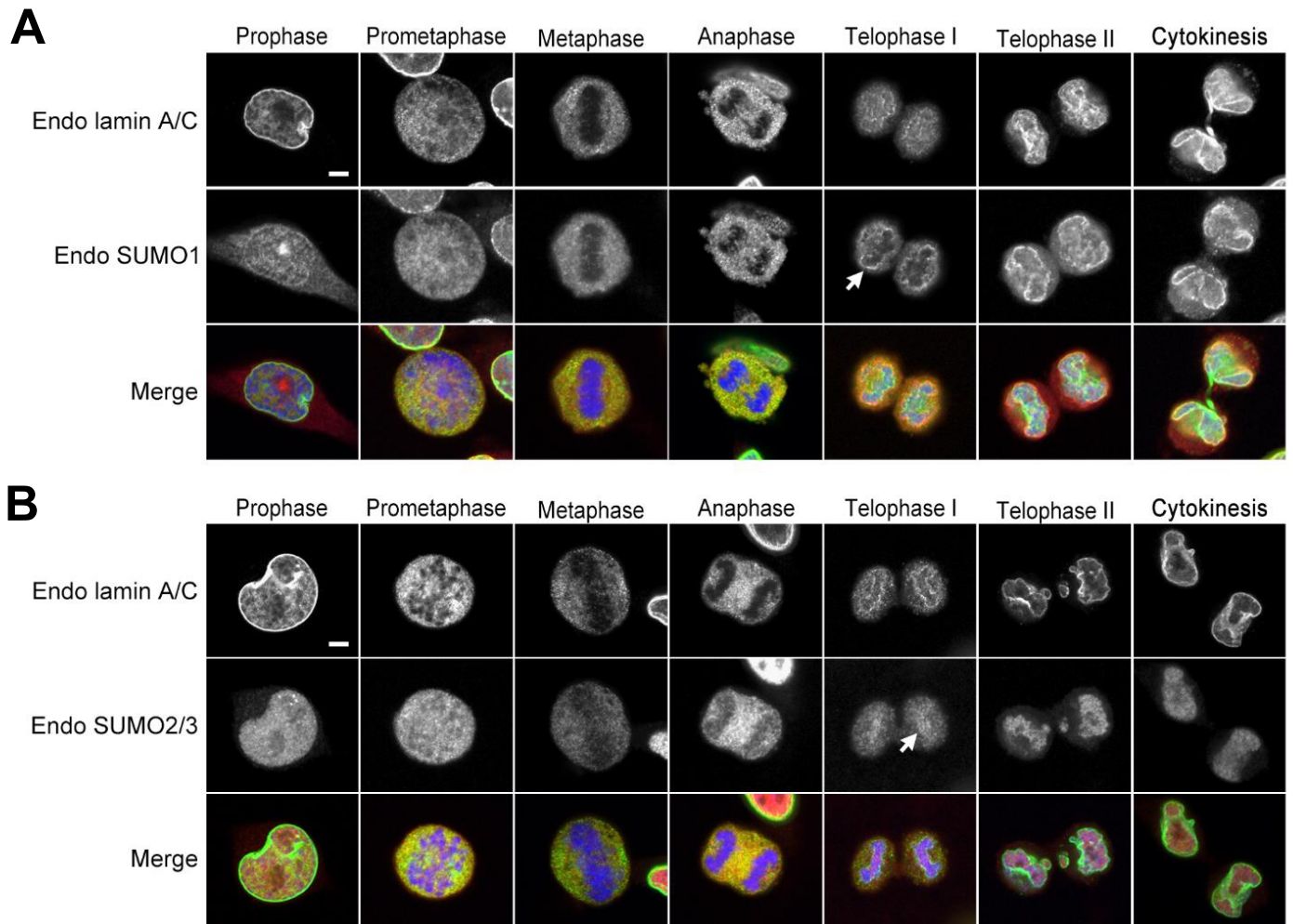


Fig. 8. Lamin A/C colocalizes with SUMO2/3 on telophase chromosomes. HeLa cells were double-stained with anti-lamin A/C (green) and anti-SUMO1 (A; red) or anti-SUMO2/3 (B; red) antibodies. The confocal images depict cells at each stage of mitosis. DNA was stained with Hoechst 33258 dye (blue). Bar, 5 μ m. The images are representative of cells examined in two independent experiments ($n > 3$ for each mitosis stage).

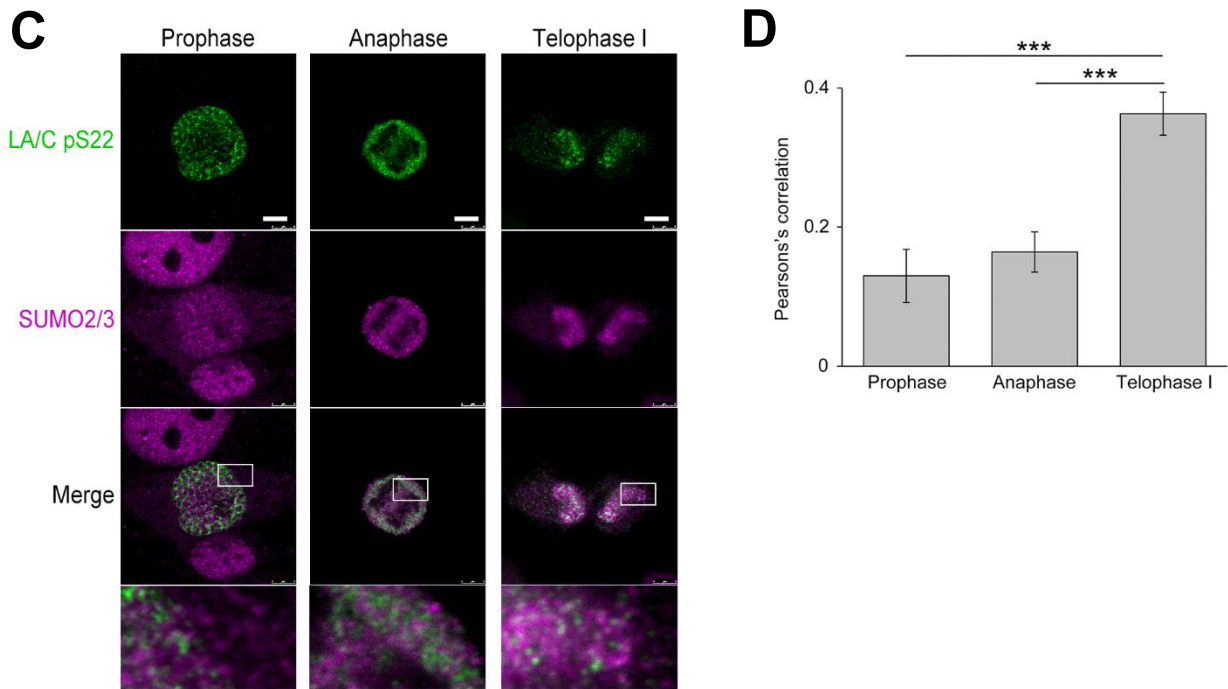


Fig. 8. Lamin A/C colocalizes with SUMO2/3 on telophase chromosomes. (C) HeLa cells were synchronized in mitosis using a nocodazole block. At 1.5 h after release from mitotic arrest, cells were subjected to immunofluorescence staining using antibodies specific to lamin A/C phosphorylated at Ser22 (LA/C pS22) and to SUMO2/3 (magenta). Representative images of cells during prophase, anaphase, or in telophase I are shown. Enlarged images within the white rectangle are shown in bottom panels. Partial colocalization of the LA/C pS22 and SUMO2/3 signals (white color) was observed in cells in telophase I. Bar, 5 μ m. (D) Analysis of colocalization of LA/C pS22 and SUMO2/3 signals in cells during prophase, anaphase, or in telophase I. The means \pm standard errors of the mean (SEM) of the Pearson's correlation coefficient from cells (prophase, 9 cells; anaphase, 7 cells; telophase I, 10 cells) are provided. *** $p < 0.0005$.

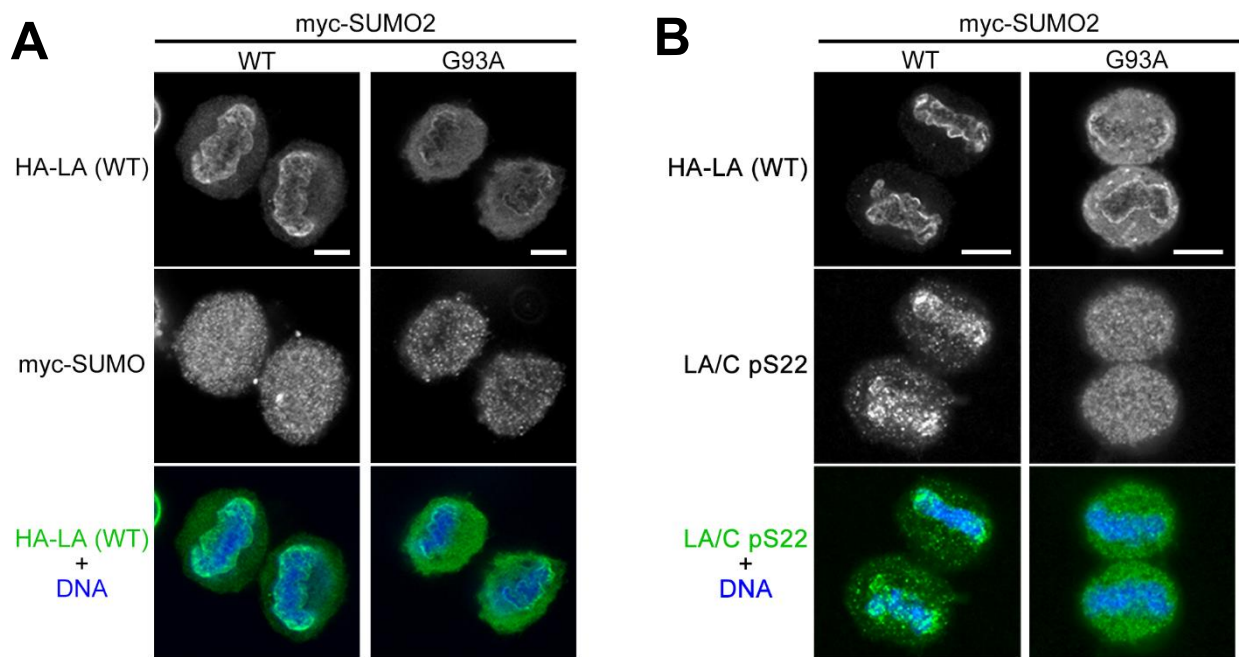


Fig. 9. Effect of the conjugation-defective small ubiquitin-related modifier 2 (SUMO2) mutant on lamin A localization. (A) HeLa cells were simultaneously transfected with plasmids expressing HA-lamin A and either wild type (WT) SUMO2 (n = 9) or the conjugation-defective SUMO2 (G93A) mutant (n = 4). At 28 h after transfection, the cells were fixed and double-stained with anti-HA (green) and anti-myc antibodies. DNA was stained with Hoechst 33258 dye (blue). Confocal images of cells in telophase I are shown. Bar, 5 μ m. (B) HeLa cells were simultaneously transfected with plasmids expressing HA-lamin A and either WT SUMO2 (n = 11) or SUMO2 (G93A) (n = 5). At 28 h after transfection, the cells were fixed and double-stained with anti-HA and anti-phosphorylated lamin A/C (Ser22) (green) antibodies. DNA was stained with Hoechst 33258 dye (blue). Confocal images of cells in telophase I are shown. Bar, 5 μ m.

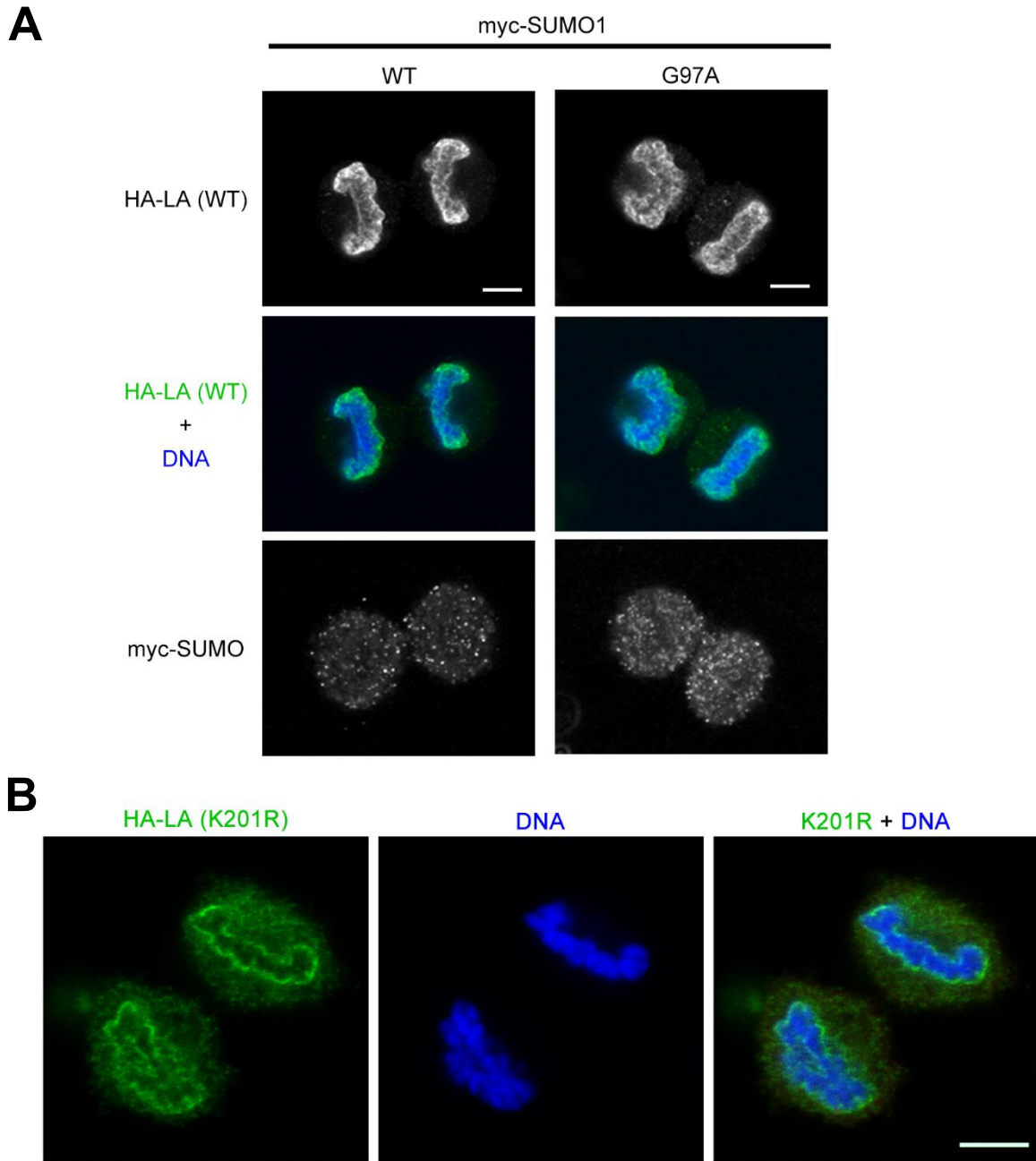


Fig. 10. Effect of the conjugation-defective small ubiquitin-related modifier 1 (SUMO1) mutant on the localization of lamin A and the lamin A K201R mutant in telophase I. (A) HeLa cells were simultaneously transfected with plasmids expressing HA-lamin A and either myc-wild type (WT) SUMO1 or the conjugation-defective myc-SUMO1 (G97A) mutant. At 28 h after transfection, the cells were fixed and stained with HA- (green) and myc-specific antibodies. DNA was stained with Hoechst 33258 dye (blue). Bar, 5 μ m. The images are representative of more than three cells. (B) HeLa cells expressing HA-lamin A K201R were subjected to immunofluorescence staining using an anti-HA antibody (HA-LA [K201R]; green). DNA was stained with Hoechst 33258 dye. Bar, 5 μ m. The images are representative of more than three cells.

Additionally, chromosomal accumulation of lamin A pS22 was not observed in cells expressing SUMO2 (G93A) (Fig. 9B). Notably, however, expression of the conjugation-defective myc-SUMO1 (G97A) mutant had no effect on lamin A localization during telophase (Fig. 10A). Together, these results indicate that the chromosomal accumulation of lamin A pS22 during telophase may depend on the presence of a SUMO2-modified protein(s) that is already associated with the chromosomes.

3-6. Discussion

In this report, I demonstrated that the C-terminal 156 amino acids of lamin A, which contains an NLS and an Ig-fold domain, are involved in the normal accumulation of lamin A on telophase chromosomes. These findings are therefore consistent with those of a previous report demonstrating that this region of lamin A is responsible for chromatin or DNA binding (Taniura et al., 1995; Stierlé et al., 2003). I also provided evidence that SIM3, located within the Ig-fold, plays a crucial role in the spatiotemporal regulation of dephosphorylation of lamin A during telophase. To the best of our knowledge, this is the first report of a SUMO-SIM interaction that is involved in the spatiotemporal regulation of dephosphorylation.

Analysis of an alignment of various SIM-containing regions revealed that the majority of these motifs contain a stretch of acidic amino acids adjacent to the SIM. In contrast, there are no neighboring acidic amino acid stretches near the N- or C-terminal region of the SIM3 motif of lamin A. A similar type of SIM was reported in TRAF and TNF receptor-associated protein (TTRAP) (Hecker et al., 2006). Interestingly, TTRAP was shown to interact with SUMO2 preferentially to SUMO1. Consistent with these findings, our GST pull-down experiments showed that lamin A exhibited higher affinity for SUMO2/3 than for SUMO1 *in vitro*. Together, these findings suggest that the absence of stretches of acidic amino acids adjacent to the SIM may promote the preference for SUMO2 in both TTRAP and lamin A.

Detailed immunofluorescence analyses revealed that phosphorylated lamin A/C transiently accumulated on condensed chromosomes during early telophase, after which the majority of the signal quickly disappeared prior to the beginning of cytokinesis. Interestingly, nuclear lamina reorganization occurred shortly after the disappearance of phosphorylated lamin A from the telophase chromosomes, implying that dephosphorylation of lamin A/C may occur on the condensed chromosomes during early telophase. I also found that mutation of SIM3 abolished the localization of lamin A to telophase chromosomes *in vivo*, as well as the interaction between lamin A and SUMO2 *in vitro*. Moreover, I found that this mutation caused a delay or defect in lamin A dephosphorylation, which is required for the assembly of the nuclear lamina. These

results suggest that this delay/defect is the result of the failed association between lamin A and the chromosomes during telophase I.

My data also demonstrate that inhibition of SUMOylation via expression of the dominant-negative SUMO2 (G93A) mutant impaired the chromosomal targeting of lamin A during early telophase. Considering that previous reports have shown that lamin A is modified with SUMO2 at K201 (Zhang and Sarge, 2008; Moriuchi et al., 2014), it is possible that defects in the SUMOylation of the lamin A polypeptide itself caused this phenotype. However, because the K201R lamin A mutant, which is not SUMOylated at K201, exhibited normal assembly on telophase chromosomes (Fig. S4B), I excluded this possibility. Therefore, it is probable that the SUMO-interacting function of SIM3 is responsible for the binding of lamin A to telophase chromosomes. Moreover, I hypothesize that phosphorylated lamin A is recruited to telophase chromosomes through an interaction with a chromatin-binding protein(s) modified with SUMO2, and is subsequently dephosphorylated on the chromosomes during telophase; however, the identification of such a recruiting protein is necessary to further characterize the mechanism governing the organization of the nuclear lamina at the end of mitosis. Recent quantitative proteomics approaches, such as stable isotope labeling by amino acids in cell culture (SILAC), using cells synchronized at different cell-cycle stages have uncovered SUMO2/3-modified proteins during mitosis that contain several chromatin-binding factors (Schimmel et al., 2014; Schou et al., 2014). Indeed, Cubeñas-Potts et al. (2015) purified and identified 149 distinct SUMO2/3-modified proteins from mitotic chromosomes. In addition, I have considered several other putative SUMOylation-dependent lamin A-binding proteins: BAF, emerin, PP1 γ , and the phosphatase interactor Repo-Man (Moorhead et al., 2007; Haraguchi et al., 2008). Interestingly, each of these candidates contains a consensus amino acid sequence for SUMOylation. Notably, in contrast to our conclusion regarding SIM3 function, structural analyses of the Ig-fold of lamin A by NMR and X-ray crystallography imply that SIM3 is located within a β strand that contributes to the formation of a β sandwich that exhibits low solvent accessibility (Krimm et al., 2002; Dhe-Paganon et al., 2002). I am therefore interested in the molecular mechanism underlying the interaction between SIM3 and SUMO or SUMOylated protein(s). I speculate that post-translational modification of lamin A, such as mitosis-

specific phosphorylation and/or interaction with certain binding proteins, as mentioned above, results in a conformational change that increases the solvent accessibility of the SIM3 region. To address this contradiction, identification of factor(s) that bind to lamin A through SIM-SUMO interaction and detailed analyses of these binding properties are needed.

It was previously reported that the reassembly of A- and B-type lamins is governed by distinct mechanisms (Haraguchi et al., 2008). Consistent with this finding, I observed that the reassembly of lamin B was not affected by expression of the SIM3 mutant through the end of cytokinesis. SIM3, which is uniquely present in the A-type lamins, may therefore contribute to the regulation of lamin A-specific reassembly. Meanwhile, I observed abnormal organization of the nuclear envelope, including lamin B and the nuclear pore complex, in HeLa cells expressing the SIM3 mutant after cell division. These results support previous reports indicating that the organization of nuclear envelope complexes is completed in early G1 (Clever et al., 2013; Kind et al., 2013) through direct and/or indirect interactions among LEM-domain proteins, nuclear pore complex proteins, A- and B-type lamins, and chromatin (Shumaker et al., 2001; Clever et al., 2013).

In conclusion, I have demonstrated that phosphorylated lamin A associates with telophase chromosomes via an interaction between SIM3 and a chromatin-binding protein(s) modified with SUMO2, after which the protein is dephosphorylated (Fig. 11). My findings indicate that this SUMO-SIM interaction facilitates the reassembly of the nuclear lamina around the daughter chromosomes, and thus provide novel insights into this important process.

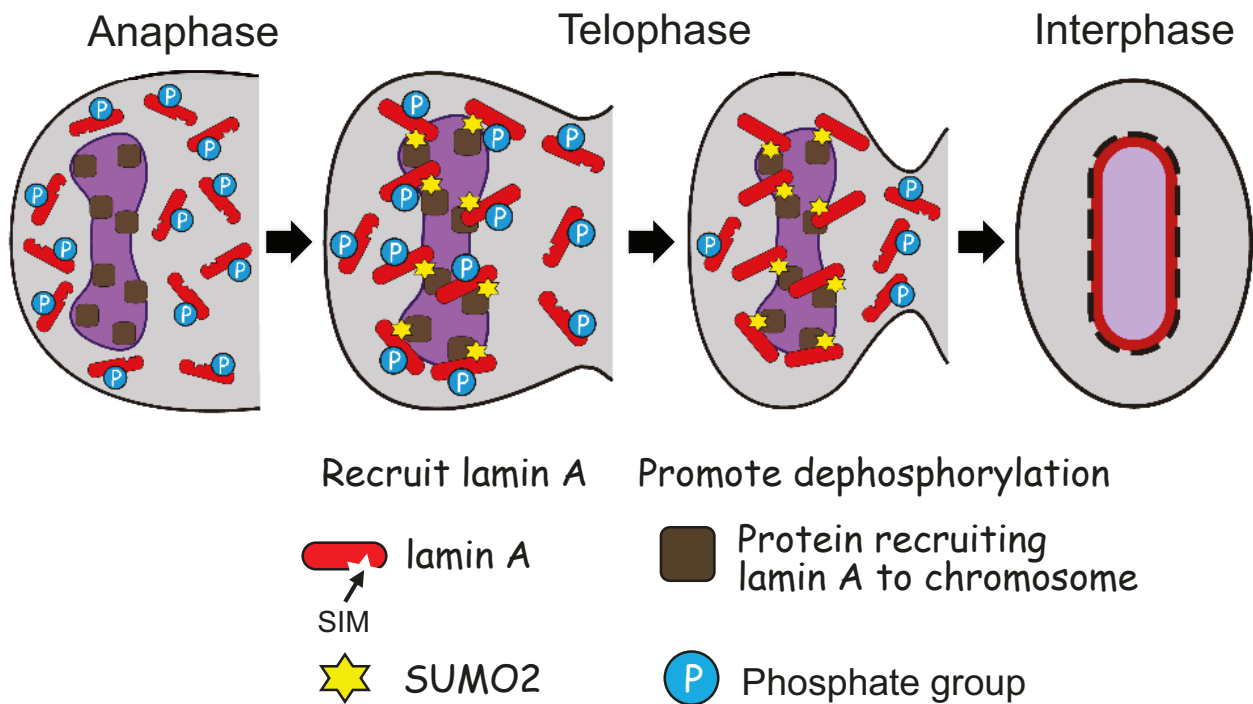


Figure 11. Model of nuclear lamina reassembly during telophase.

Phosphorylated lamin A disperses in cytoplasm during anaphase. A protein recruiting lamin A to chromosome is modified with SUMO2/3 and then recruit phosphorylated lamin A to telophase chromosomes. Phosphorylated lamin A is dephosphorylated on telophase chromosomes. The nuclear lamina is reorganized after mitotic exit.

3-7. References

1. Agostinho, M., V. Santos, F. Ferreira, R. Costa, J. Cardoso, I. Pinheiro, J. Rino, E. Jaffray, R.T. Hay, and J. Ferreira. (2008). Conjugation of human topoisomerase 2 alpha with small ubiquitin-like modifiers 2/3 in response to topoisomerase inhibitors: cell cycle stage and chromosome domain specificity. *Cancer Res.* **68**, 2409–2418.
2. Andrés, V., and J.M. González. (2009). Role of A-type lamins in signaling, transcription, and chromatin organization. *J. Cell Biol.* **187**, 945–957.
3. Azuma, Y., A. Arnaoutov, T. Anan, and M. Dasso. (2005). PIASy mediates SUMO-2 conjugation of Topoisomerase-II on mitotic chromosomes. *EMBO J.* **24**, 2172–2182.
4. Carron, C., S. Balor, F. Delavoie, C. Plisson-Chastang, M. Faubladiet, P.-E. Gleizes, and M.-F. O’Donohue. (2012). Post-mitotic dynamics of pre-nucleolar bodies is driven by pre-rRNA processing. *J. Cell Sci.* **125**, 4532–4542.
5. Clever, M., Y. Mimura, T. Funakoshi, and N. Imamoto. (2013). Regulation and coordination of nuclear envelope and nuclear pore complex assembly. *Nucleus.* **4**, 105–114.
6. Dechat, T., S.A. Adam, P. Taimen, T. Shimi, and R.D. Goldman. (2010). Nuclear lamins. *Cold Spring Harb. Perspect. Biol.* **2**, a000547.
7. Dhe-Paganon, S., E.D. Werner, Y.-I. Chi, and S.E. Shoelson. (2002). Structure of the globular tail of nuclear lamin. *J. Biol. Chem.* **277**, 17381–17384.
8. Georgatos, S.D., A. Pырpasopoulou, and P.A. Theodoropoulos. (1997). Nuclear envelope breakdown in mammalian cells involves stepwise lamina disassembly and microtubule-drive deformation of the nuclear membrane. *J. Cell Sci.* **110**, 2129–2140.
9. Gómez-del Arco, P., J. Koipally, and K. Georgopoulos. (2005). Ikaros SUMOylation: switching out of repression. *Mol. Cell. Biol.* **25**, 2688–2697.
10. Goss, V.L., B.A. Hocevar, L.J. Thompson, C.A. Stratton, D.J. Burns, and A.P.

- Fields. (1994). Identification of nuclear beta II protein kinase C as a mitotic lamin kinase. *J. Biol. Chem.* **269**, 19074–19080.
11. Haraguchi, T., T. Kojidani, T. Koujin, T. Shimi, H. Osakada, C. Mori, A. Yamamoto, and Y. Hiraoka. (2008). Live cell imaging and electron microscopy reveal dynamic processes of BAF-directed nuclear envelope assembly. *J. Cell Sci.* **121**, 2540–2554.
 12. Hashimoto, T., H. Segawa, M. Okuno, H. Kano, H. Hamaguchi, T. Haraguchi, Y. Hiraoka, S. Hasui, T. Yamaguchi, F. Hirose, and T. Osumi. (2012). Active involvement of micro-lipid droplets and lipid-droplet-associated proteins in hormone-stimulated lipolysis in adipocytes. *J. Cell Sci.* **125**, 6127–6136.
 13. Heald, R., and F. McKeon. (1990). Mutations of phosphorylation sites in lamin A that prevent nuclear lamina disassembly in mitosis. *Cell.* **61**, 579–589.
 14. Hecker, C.-M., M. Rabiller, K. Haglund, P. Bayer, and I. Dikic. (2006). Specification of SUMO1- and SUMO2-interacting motifs. *J. Biol. Chem.* **281**, 16117–16127.
 15. Hocevar, B.A., D.J. Burns, and A.P. Fields. (1993). Identification of protein kinase C (PKC) phosphorylation sites on human lamin B. Potential role of PKC in nuclear lamina structural dynamics. *J. Biol. Chem.* **268**, 7545–7552.
 16. Kind, J., L. Pagie, H. Ortazobkoyun, S. Boyle, S.S. de Vries, H. Janssen, M. Amendola, L.D. Nolen, W.A. Bickmore, and B. van Steensel. (2013). Single-cell dynamics of genome-nuclear lamina interactions. *Cell.* **153**, 178–192.
 17. Krimm, I., C. Ostlund, B. Gilquin, J. Couprie, P. Hossenlopp, J.-P. Mornon, G. Bonne, J.-C. Courvalin, H.J. Worman, and S. Zinn-Justin. (2002). The Ig-like structure of the C-terminal domain of lamin A/C, mutated in muscular dystrophies, cardiomyopathy, and partial lipodystrophy. *Structure.* **10**, 811–823.
 18. Li, Y., H. Wang, S. Wang, D. Quon, Y.-W. Liu, and B. Cordell. (2003). Positive and negative regulation of APP amyloidogenesis by sumoylation. *Proc. Natl. Acad. Sci. U. S. A.* **100**, 259–264.

19. Lin, D.-Y., Y.-S. Huang, J.-C. Jeng, H.-Y. Kuo, C.-C. Chang, T.-T. Chao, C.-C. Ho, Y.-C. Chen, T.-P. Lin, H.-I. Fang, C.-C. Hung, C.-S. Suen, M.-J. Hwang, K.-S. Chang, G.G. Maul, and H.-M. Shih. (2006). Role of SUMO-interacting motif in Daxx SUMO modification, subnuclear localization, and repression of sumoylated transcription factors. *Mol. Cell.* **24**, 341–354.
20. Minty, A., X. Dumont, M. Kaghad, and D. Caput. (2000). Covalent modification of p73alpha by SUMO-1. Two-hybrid screening with p73 identifies novel SUMO-1-interacting proteins and a SUMO-1 interaction motif. *J. Biol. Chem.* **275**, 36316–36323.
21. Moir, R.D., M. Yoon, S. Khuon, and R.D. Goldman. (2000). Nuclear Lamins a and B1 : Different Pathways of Assembly during Nuclear Envelope Formation in Living Cells. *J. Cell Biol.* **151**, 1155–68.
22. Moorhead, G.B.G., L. Trinkle-Mulcahy, and A. Ulke-Lemée. (2007). Emerging roles of nuclear protein phosphatases. *Nat. Rev. Mol. Cell Biol.* **8**, 234–244.
23. Moriuchi, T., T. Muraoka, K. Mio, T. Osumi, and F. Hirose. (2014). Long-term expression of the lamin A mutant associated with dilated cardiomyopathy induces senescence. *Genes Cells.* **19**, 901–918.
24. Parry, D.A., J.F. Conway, and P.M. Steinert. (1986). Structural studies on lamin. Similarities and differences between lamin and intermediate-filament proteins. *Biochem. J.* **238**, 305–308.
25. Peter, M., J. Nakagawa, M. Dorée, J.C. Labbé, and E.A. Nigg. (1990). In vitro disassembly of the nuclear lamina and M phase-specific phosphorylation of lamins by cdc2 kinase. *Cell.* **61**, 591–602.
26. Savino, T.M., J. Gébrane-Younès, J. De Mey, J.B. Sibarita, and D. Hernandez-Verdun. (2001). Nucleolar assembly of the rRNA processing machinery in living cells. *J. Cell Biol.* **153**, 1097–1110.
27. Schimmel, J., K. Eifler, J.O. Sigurðsson, S.A.G. Cuijpers, I.A. Hendriks, M. Verlaan-de Vries, C.D. Kelstrup, C. Francavilla, R.H. Medema, J. V. Olsen, and A.C.O. Vertegaal. (2014). Uncovering SUMOylation dynamics during cell-cycle

- progression reveals FoxM1 as a key mitotic SUMO target protein. *Mol. Cell.* **53**, 1053–1066.
28. Schou, J., C.D. Kelstrup, D.G. Hayward, J. V. Olsen, and J. Nilsson. (2014). Comprehensive identification of SUMO2/3 targets and their dynamics during mitosis. *PLoS One.* **9**, e100692.
 29. Shumaker, D.K., K.K. Lee, Y.C. Tanhehco, R. Craigie, and K.L. Wilson. (2001). LAP2 binds to BAF.DNA complexes: requirement for the LEM domain and modulation by variable regions. *EMBO J.* **20**, 1754–1764.
 30. Song, J., L.K. Durrin, T.A. Wilkinson, T.G. Krontiris, and Y. Chen. (2004). Identification of a SUMO-binding motif that recognizes SUMO-modified proteins. *Proc. Natl. Acad. Sci. U. S. A.* **101**, 14373–14378.
 31. Steen, R.L., S.B. Martins, K. Taskén, and P. Collas. (2000). Recruitment of protein phosphatase 1 to the nuclear envelope by A-kinase anchoring protein AKAP149 is a prerequisite for nuclear lamina assembly. *J. Cell Biol.* **150**, 1251–1261.
 32. Stierlé, V., J. Couprie, C. Ostlund, I. Krimm, S. Zinn-Justin, P. Hossenlopp, H.J. Worman, J.-C. Courvalin, and I. Duband-Goulet. (2003). The carboxyl-terminal region common to lamins A and C contains a DNA binding domain. *Biochemistry.* **42**, 4819–4828.
 33. Taniura, H., C. Glass, and L. Gerace. (1995). A chromatin binding site in the tail domain of nuclear lamins that interacts with core histones. *J. Cell Biol.* **131**, 33–44.
 34. Thompson, L.J., M. Bollen, and A.P. Fields. (1997). Identification of protein phosphatase 1 as a mitotic lamin phosphatase. *J. Biol. Chem.* **272**, 29693–29697.
 35. Ward, G.E., and M.W. Kirschner. (1990). Identification of cell cycle-regulated phosphorylation sites on nuclear lamin C. *Cell.* **61**, 561–77.
 36. Yamasaki, M., N. Hashiguchi, T. Tsukamoto, and T. Osumi. (1998). Variant forms of green and blue fluorescent proteins adapted for the use in mammalian cells. *Bioimages.* **6**, 1–7.
 37. Yamashita, D., T. Yamaguchi, M. Shimizu, N. Nakata, F. Hirose, and T. Osumi.

- (2004). The transactivating function of peroxisome proliferator-activated receptor γ is negatively regulated by SUMO conjugation in the amino-terminal domain. *Genes to Cells* **9**, 1017-1029.
38. Zhang, X.-D., J. Goeres, H. Zhang, T.J. Yen, A.C.G. Porter, and M.J. Matunis. (2008). SUMO-2/3 modification and binding regulate the association of CENP-E with kinetochores and progression through mitosis. *Mol. Cell*. **29**, 729–741.
39. Zhang, Y.-Q., and K.D. Sarge. (2008). Sumoylation regulates lamin A function and is lost in lamin A mutants associated with familial cardiomyopathies. *J. Cell Biol.* **182**, 35–39.
40. Zhao, Q., Y. Xie, Y. Zheng, S. Jiang, W. Liu, W. Mu, Z. Liu, Y. Zhao, Y. Xue, and J. Ren. (2014). GPS-SUMO: a tool for the prediction of sumoylation sites and SUMO-interaction motifs. *Nucleic Acids Res.* **42**, 325–330.

4. Acknowledgements

I would like to thank Drs. Fumiko Hirose and Takashi Osumi throughout my work. Their supports are too grateful for words. I also would like to thank members of Cell and Molecular biology laboratory.

I thank Dr. Hirofumi Komori (Kagawa University) for the expressing plasmid pET47b, Dr. Hiroyuki Miyoshi for lentivirus vector (Riken) and Dr. Kazuhiro Mio for lamin A paracrystals formation experiment.